Methods For Aiding Height Determination In Pseudolite-Based Reference Systems Using Batch Least-Squares Estimation

THESIS

John Harold Robert Amt,

AFIT/GE/ENG/06-03

DEPARTMENT OF THE AIR FORCE
AIR UNIVERSITY

AIR FORCE INSTITUTE OF TECHNOLOGY

Wright-Patterson Air Force Base, Ohio

The views expressed in this thesis are those of the author and do not reflect the official policy or position of the United States Air Force, Department of Defense, or the United States Government

AFIT/GE/ENG/06-03

Methods For Aiding Height Determination In Pseudolite-Based Reference Systems Using Batch Least-Squares Estimation

THESIS

Presented to the Faculty

Department of Electrical and Computer Engineering

Graduate School of Engineering and Management

Air Force Institute of Technology

Air University

Air Education and Training Command

In Partial Fulfillment of the Requirements for the

Degree of Master of Science in Electrical Engineering

John Harold Robert Amt, B.S.E.E.

March 2006

AFIT/GE/ENG/06-03

Methods For Aiding Height Determination In Pseudolite-Based Reference Systems Using Batch Least-Squares Estimation

John Harold Robert Amt, B.S.E.E.

Approved:

/signed/	3 Mar 2006
Dr. John Raquet (Chairman)	date
/signed/	3 Mar 2006
Dr. Meir Pachter (Member)	date
/signed/	3 Mar 2006
Lt. Col. Juan Vasquez (Member)	date

Abstract

There are many situations in which GPS is either unable to provide the desired level of accuracy or is unavailable. Use of a pseudolite-based reference system for navigation can be a means for positioning during these times. While there are advantages in using a pseudolite-based reference system, there are still implementation issues and deficiencies that must be addressed. In many cases a pseudolite system with ground based transmitters has difficulty in determining the height of the receiver accurately. This is due to the poor vertical observability inherent in the geometry of the system. A common approach in naval applications for solving the problem of poor vertical observability is to use a height constraint, which is well known when travelling on a surface of water. For a ground-based vehicle, knowledge of the surface topography can be obtained, but cannot be readily used in the same manner as marine cases, since the height is often a varying function of position.

This research investigates and develops five methods of incorporating the known surface topography in a non-linear batch least squares estimation algorithm using carrier-phase measurements from pseudolites. The floating point carrier-phase ambiguities are estimated in this process. Real and simulated data sets are used to evaluate the performance of the five algorithms. In simulation, all methods performed equivalently well on a flat surface. When simulating a hill, constraining the solution to lie in a plane tangent to the surface topography appeared to aid the solution with the best knowledge of the terrain. Use of a pseudo-measurement, a commonly used approach, did not provide the best results, and indicates the inadequacy of using this method for pseudolite-based systems. Results using data from a real system on a ground-based vehicle demonstrated sub-decimeter level positioning accuracy in all three dimensions.

Acknowledgements

First and foremost, I want to thank the Lord for all the loved ones, friends, and opportunities He has blessed me with. I want thank my parents for always being there for me and providing the best family anyone could ask for. I want to thank Dr. Raquet for his guidance and support. Saving the best for last, I want to thank my one true love for her support and patience. It is for us that I started this endeavor and only with her that I could have completed it. I will always love you.

John Harold Robert Amt

Table of Contents

Page

Page

List of Figures

List of Tables

List of Symbols

Symbol		Page
ρ	Pseudorange measurement	16
r	True Range	16
c	Speed of Light	16
δt_u	Receiver clock error	16
δt_{sv}	Satellite clock error	16
T	Tropospheric delay	16
I	Ionosperic delay	16
m_ρ	Multipath pseudorange error	16
v_ρ	Pseudorange Receiver Noise	16
ϕ	Carrier-Phase Measurement	17
λ	Carrier wavelength	17
m_ϕ	Carrier-phase error due to Multipath	17
v_ϕ	Carrier-phase error due to Receiver Noise	17
N	Carrier-phase ambiguity	17
$\mathbf{z}$	Measurement vector	21
m	Number of measurements	21
$\mathbf{H}$	Measurement matrix	21
$\mathbf{x}$	Unknown State Vector	21
n	number of states	21
$\hat{\mathbf{x}}$	State Estimate Vector	21
$\mathbf{R}$	Measurement Noise Covariance Matrix	22
$\hat{\mathbf{x}}_o$	Initial State Estimate	23
$\hat{\mathbf{x}}_c$	Corrected State Estimate	23
$\hat{\mathbf{x}}$	Current State Estimate	23
$\Delta\mathbf{z}$	Measurement Residual	23
$\Delta\mathbf{x}$	Error in State Estimate	24

List of Abbreviations

Abbreviation		Page
GPS	Global Positioning System	1
DGPS	Differential GPS	1
INS	Inertial Navigation System	1
USAF	United States Air Force	2
CIGTF	Central Inertial Guidance Test Facility	2
AFB	Air Force Base	2
EGI	Embedded GPS/INS	2
CRS	CIGTF Reference System	2
LSE	Least Squares Estimation	7
SVD	Singular Value Decomposition	8
SNAP	Satellite Navigation and Positioning Group	11
C/A	Coarse-Acquisition	15
BPSK	Bi-Phase Shift Key	15
SNR	Signal-to-Noise Ratio	16
LAMBDA	Least squares AMbiguity Decorrelation Algorithm	18
FASF	Fast Ambiguity Search Filter	18
wrt	with respect to	21
WLS	Weighted Least Squares	22
ILS	Iterative Least Squares	23
ENU	East North UP	39
ECEF	Earth Centered Earth Fixed	40
DTED	Digital Terrain Elevation Data	86

Methods For Aiding Height Determination In Pseudolite-Based Reference Systems Using Batch Least-Squares Estimation

I. Introduction

1.1 Motivation

The Global Positioning System (GPS) has become an unparalleled aid in navigation. GPS was created as a military program with limited civilian use. Since becoming operational in 1993, civilian use has grown rapidly throught the world. Not just used for positioning, GPS gives accurate timing capabilities which has made it a cornerstone of countless civil systems.

With the positioning now commonplace with GPS, it has become a fight to squeeze as much capability from GPS as possible. Research in both the civilian and military sectors are attempting to meet the addiction of accurate positioning. Accuracy is addicting. Once accurate positions to meter level has been attained, it is unthinkable to stop there. Countless applications are now being considered that require increasingly higher precision. Many systems requiring high accuracy often require robustness as well. Availability of GPS, at first blush, seems all encompassing. It is all over the world. But looking closer, GPS is much more fragile than initially thought. Accuracy of solutions with an un-obstructed sky are still highly dependent on the satellite geometry. With any occlusion of the sky by obstacles, there can be significant loss of needed accuracy. Research has found many answers to these problems. Differential GPS (DGPS), carrier-phase ambiguity resolution, and augmented GPS have all boosted the accuracy and robustness of GPS based navigation. Many forms of DGPS now exist to aid the accuracy of GPS navigation. Integrated GPS systems primarily combine GPS with an inertial navigation system (INS) and create

a more robust system. Despite these improvements new demands require even more of GPS.

A flight navigation system demands some of the highest requirements in navigation. The United States Air Force (USAF) is interested in applications that need accuracy within tens of centimeters or less. This accuracy must be maintained with a very high level of robustness. A loss in accuracy for even a short time could be catastrophic in a flight system. This brings the problem of GPS jamming into view. While GPS could provide the desired accuracy, it cannot provide the robustness to jamming that is required.

Development of systems operating in GPS jamming environments poses another problem. How are these systems tested? A truth reference must have an accuracy at least an order of magnitude better than the system under test. In the past systems were tested while jamming a single GPS frequency, allowing the truth reference system to use the second available frequency for its positioning. In reality the enemy will jam both GPS frequencies. This requires that new systems be tested in this environment. It also requires that the flight test reference system also function under dual frequency jamming.

The 746th Test Squadron's Central Inertial Guidance Test Facility (CIGTF), Holloman Air Force Base (AFB), NM tests and evaluates new flight navigation systems. The current flight reference system at the Holloman AFB incorporates an Embedded GPS/INS (EGI), a second GPS receiver, a second INS, and a transponder/interrogator. This system is called the CIGTF Reference System (CRS) [14]. In the past, the test facility was able to test the robustness of GPS based flight reference systems in the presence of single frequency jamming. This testing was good for research purposes, but again does not test the situation that will most likely occur in reality. Currently the 746th does not have the capability to maintain a highly accurate (near centimeter level) truth reference under dual-frequency GPS jamming conditions.

A new flight test reference system is needed that can meet the demands of the future. This reference system must not rely on GPS, so that systems designed to operate in dual frequency jamming can be tested adequately. Furthermore, the accuracy of the system must be at least on the order of centimeters. A new technology holds the answer to creating this reference system.

Pseudo-Satellites, also called pseudolites, are transmitters that generate a GPS-like signal [10]. The new reference system will be a pseudolite based reference system. This system will use only pseudolites to create a GPS-like environment. Being able to tailor the characteristics of the pseudolites will allow the reference system to operate on a frequency other than GPS. Signals used by the truth reference system will now be unaffected by the jamming used to simulate hostile conditions for the system under test. Using pseudolites will solve the problem, but will naturally entail new issues that research must overcome.

Previous research has simulated the environment of a pseudolite based reference system [8]. The next phase of research is creation of a real system. Implementation of a proof-of-concept is underway using road tests. While road tests are only a stepping stone to creating a flight reference system, which inspired this research, there is a large amount of ground based positioning that requires high accuracy and the ability to function in a hostile environment. Thus solving the problems of ground based pseudolite positioning is extremely important.

1.2 Problem Definition

There are inherent problems that arise when using ground based pseudolites. The greatest of these lies in the geometry deficiencies. With all the transmitters near the ground there is low observability in the vertical direction. This must be overcome to gain three-dimensional accuracies on the order of centimeters.

Suppose the position of a static receiver is being estimated using pseudoranges. The known location of the receiver will be at the origin of some ENU reference co-

Table 1.1: Locations of pseudolites in ENU frame with the receiver at the origin. The slant angle gives the angle of the pseudolite from the horizontal plane as seen from the receiver.

PRN #	East (m)	North (m)	Up (m)	Slant Angle (deg)
1	-1000	1000	100	4.04
2	1000	-1000	10	.405
3	-1000	-1000	150	6.05
4	1000	1000	5	.203

ordinate frame. The locations of 4 pseudolites in the same ENU frame are shown in Table 1.1. The slant angles show that the pseudolites are all low on the horizon. This is a simple case that demonstrates poor vertical observability. Using least-squares estimation with single differenced pseudoranges the position of the receiver can be found with some uncertainty.

To simulate this example the true ranges were calculated and used as the pseudorange measurements. Measurement error was introduced as a simple zero-mean white, Gaussian noise on the measurements. A normally distributed random noise with strength of 1 m^2 was added to each measurement (this value was arbitrarily chosen for illustration purposes). These measurements were then used to estimate the receiver position using a simple ILS method. Estimation is done in 3-dimensions. This was repeated 1000 times to show the distribution of the solutions obtained. Figures 1.1 and 1.2 show the results. Figure 1.1 displays the 1000 estimated receiver positions. The scatter plot of solution points has been projected onto the 3 axes for easy interpretation of the errors in each direction. The vertical errors can be hundreds of meters off, despite a small amount of measurement noise. Figure 1.2 highlights on the horizontal errors. The east errors range approximately from -10 to 10 meters and the north errors from approximately -4 to 4 meters.

Having poor observability in the vertical dimension increases the horizontal errors due to the non-linear nature of this problem. Improving the vertical error will therefore improve the horizontal errors as well. If knowledge of the height is known

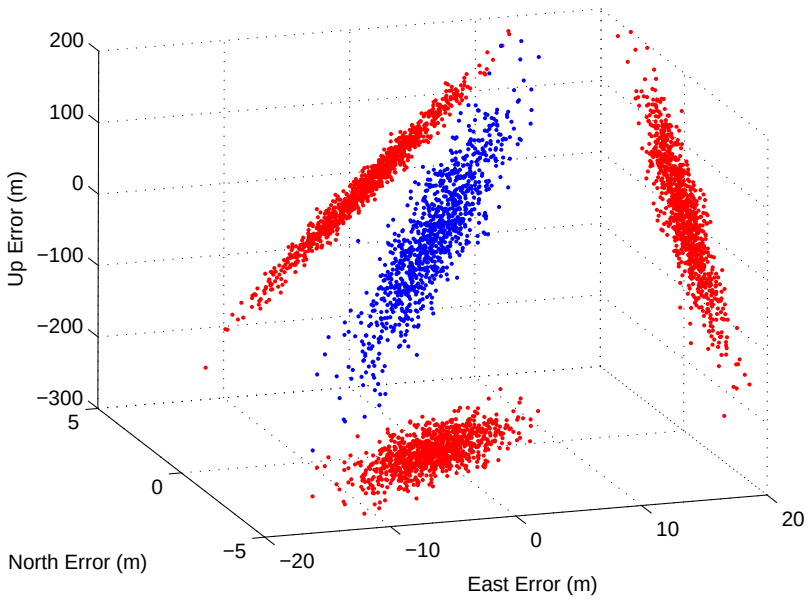

Figure 1.1: Receiver position estimation error in 3 dimensions. 1000 runs are shown with projections onto each axis (shown in red). No aiding has been done.

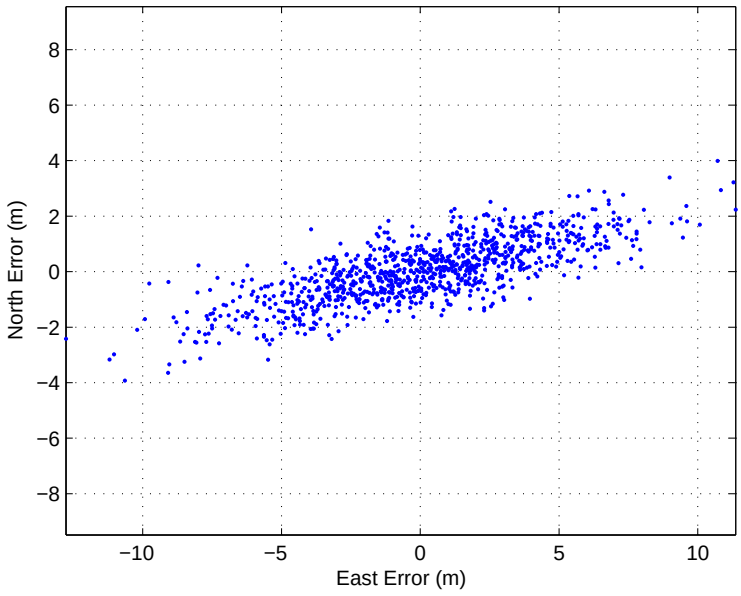

Figure 1.2: Horizontal position estimation errors with no aiding.

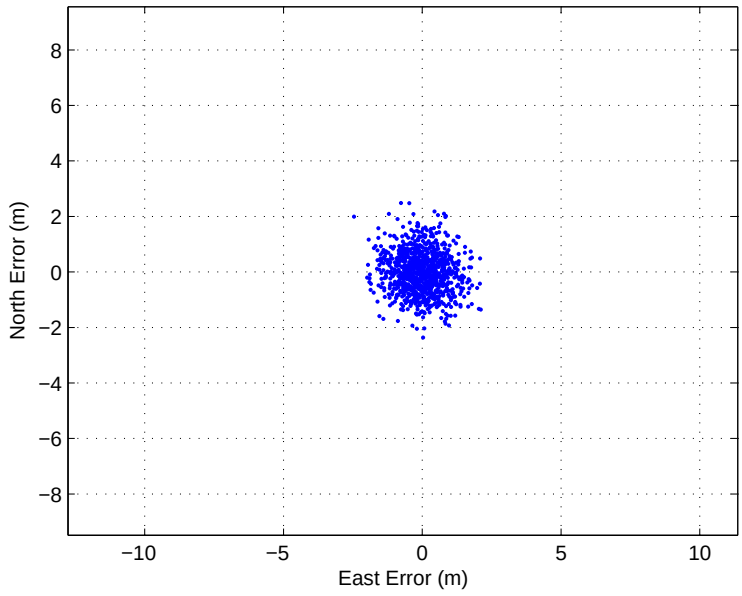

Figure 1.3: Horizontal position estimation errors. Aiding has been done.

from a source other than the given measurements this can be used to aid the solution. The simplest method is to assume the height is known. Constraining the height will allow the solution to be estimated in the horizontal plane only.

This was simulated and the results are shown in Figure 1.3. Comparison to the horizontal errors in Figure 1.2 will show a reduction of errors when height constraining is used. The east and north errors have both been reduced to ranges of -2 to 2 meters.

The previous example illustrates what simply constraining the solution to a known height can accomplish. This technique is very simple and is used in practice. Many applications allow the user to assume a receiver height.

In a ground based test the receiver height is not as intrinsically known is in some cases. The receiver is also in motion. This does not mean that information is not available. If the ground topography were known prior to the test, then knowledge of where the receiver is in the east and north directions will indicate the receiver height. Unfortunately, each direction is being estimated simultaneously. Methods of

incorporating this height information into the estimation of the position of a moving receiver must be developed.

This research focuses on evaluating different methods of incorporating the knowledge of the height into the solution. The height information is obtained from assuming that the receiver is travelling upon an unchanging surface. This surface can be surveyed prior to testing, and then used to aid the solution algorithm.

1.3 Proposed Solution

The algorithms that will be developed are all based upon using least squares estimation (LSE). Actually, a nonlinear, iterative, weighted, batch least squares estimation method will be implemented. This will address the issues in dealing with a position solution using carrier-phase measurements and the inherent ambiguities.

A surface grid will be created by using GPS to map points along the desired test trajectory. It is important to note that the GPS surveying of these points must also have centimeter level accuracy. The creation of the grid will not be affected by the GPS jamming in the test, since the grid will be formed prior to the test. In the road test conducted, no system was being tested under any GPS jamming, therefore DGPS measurements were collected during the pseudolite testing.

Several methods for integrating the information from the grid into the solution are proposed in this research:

- Method 1: Only the horizontal components of the position are estimated. The vertical height is assumed to be a known value. Once the horizontal position is known, it is used to find the corresponding vertical height on the grid. This new height is used in the next iteration as the height constraint. The solution is then iterated upon in this fashion. Thus the iterative solution is constrained to the surface grid.
- Method 2: Instead of forcing the solution to be in the horizontal plane, all three dimensions are esimated. The low observability in the vertical direction that

would normally cause the solution to be unobtainable is corrected by creating a pseudo-measurement using the GPS grid. This measurement is created much the same way as in Method 1 (by finding the corresponding height using the current horizontal position of the solution). This height is then treated as an additional measurement and is incorporated into the algorithm. Since a weighted LSE method is being used, the pseudo-measurement can be weighted very high to keep the solution very close to the actual grid.

- Method 3: Instead of assuming that the 2 horizontal directions are the best choices to constrain the system, it is possible to find the 2 best axes. By using singular value decomposition (SVD), the optimal dimension reduction can be made. Depending on the geometry of the pseudolites to the receiver, the two principal axis may be slightly different than the horizontal directions that are normally used. A state transformation is used so that the solution is found in the optimal plane based on the geometry. There will still be problems with the vertical direction. The SVD approach will only allow the solution space to be optimized, removing the direction with the least information; however, the solution is still only in 2-dimensions. The information from the grid will be incorporated by constraining the solution to lie on the known surface. Unlike Method 1 however, the solution will have been constrained to a plane that optimally incorporates the measurements. This method will incorporate the SVD approach at each epoch when forming the batch process.
- Method 4: This Method will also incorporate the SVD approach. It will comprise the same method as in method 3 but will be used on the full batch process. This will allow all the information known in the batch process to aid in finding the optimal solution space.
- Method 5: Another method similar to the SVD approach will rely upon the geometry of the GPS grid instead of the pseudolite/receiver geometry. Instead of finding a solution on a plane based upon the relative geometry of the pseudolites and receiver, the solution will find the plane that is tangent to the surface of

the pre-defined surface at the current position. In an environment that has a more dynamic surface than a flat plane, this method will allow the solution to be solved in the directions that correspond more closely to the known height surface.

1.4 Goals

The goal of this research is to implement and analyze the above mentioned methods for aiding a pseudolite-based reference system. Since real data is available, it will be used in the analysis. Simulation data will also be generated so that different surfaces and noise sources can be tested. Each method will be created and tuned to give its best performance with real data. The simulations will then be created to test each algorithm's robustness and compare them against each other.

1.5 Scope

This research will further develop the algorithms used in finding the navigation solution using a pseudolite-based reference system. The real data that has been collected is from a pseudolite test facility. The data has been collected in a moving ground vehicle. Truth trajectories were collected at the same time as the pseudolite data. The algorithms and simulations will be created in the `Matlab`® 7.0 environment.

Along with developing the algorithms mentioned above, methods to deal with real data issues are created. Methods to find carrier-phase cycle slips are addressed, since there are different problems associated with pseudolites than with normal GPS receivers. Furthermore, methods for dealing with tropospheric error are also evaluated. As will be discussed later, tropospheric error must be handled differently than in most differential GPS cases.

The pseudolites used for this research are manufactured by Locata Inc., and provide a time synchronization protocol that solves the problem of pseudolite clock errors.

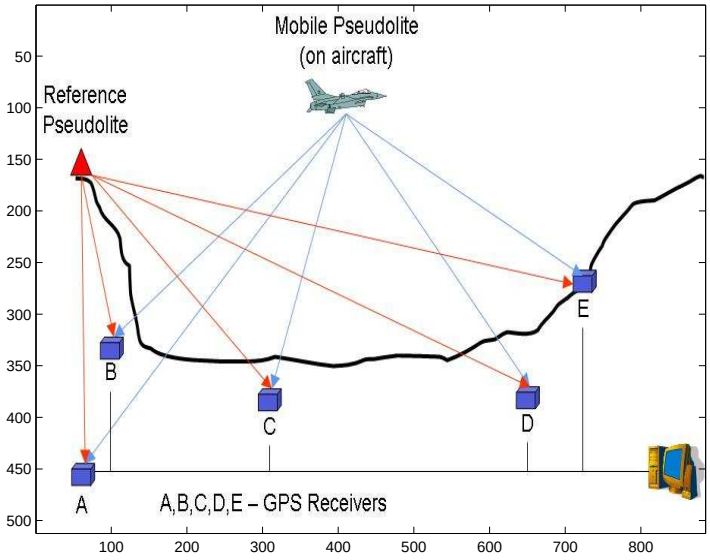

Figure 1.4: The Inverted Pseudolite Architecture.

1.6 Assumptions

The following assumptions are made in this thesis:

1. Real-time solutions are not required, because the research is directed toward the use as the truth trajectory for a flight test reference system. All data is able to be post processed.
2. The pseudolites are synchronized using the manufacturer's TimeLoc system. This eliminates the time offset that is usually inherent with pseudolites.
3. No jamming analysis is required, because the pseudolites operate at a different frequency than GPS.

1.7 Related Research

1.7.1 Inverted Pseudolite System. In April 1995, the 746th Test Squadron implemented a novel pseudolite based reference system. This system used an inverted architecture shown in Figure 1.4. In the test, a van was used to carry a pseudolite transmitter. Another pseudolite was placed on the ground as a reference signal.

With receivers placed at known locations on the ground, it is possible to implement a reference system. This research was a proof-of-concept for creating a pseudolite based reference system. It was shown to have accuracy at the decimeter level, with promise of even better accuracy with further development. A drawback is that the mobile unit does not have access to the position solution unless it is received as another signal from the ground station. Further detail can be obtained in [22]. A key finding of the research was that an accurate solution is highly dependent on accurate surveying of the reference receivers and reference pseudolite.

1.7.2 Analysis of Pseudolite Augmentation for GPS Airborne Applications. In 2002 the Satellite Navigation and Positioning Group (SNAP) presented research investigating the augmentation of pseudolites with GPS for airborne applications [15]. Implementation issues such as antenna locations and placement of the pseudolites was considered. Placement of a second antenna on the bottom of the aircraft was needed for reception of ground-based transmitters. It was found that the magnitude of the antenna offset (between the GPS and pseudolite antennas) will determine the accuracy in the attitude measurements. Pseudolites were found to significantly improve the transmitter geometry and the signal availability of a airborne navigation system. It was also found that the addition of more than 3 psedolites into the system gained only marginal improvement. The research does not investigate the deficiencies when landing, although in this research both pseudolites and GPS satellites are used.

1.7.3 Simulation of a Pseudolite Reference System. Development and simulation of a pseudolite-based reference system is given in [8,9]. The master's thesis uses the flight path of a C-12 as simulation truth data. Double differenced measurements are used as well as optimal smoothing with Kalman filters. The tropospheric error is first reduced using a modified troposphere model, and then the residual error is reduced through the differencing techniques. The final tropospheric residual error is still significant enough to be of concern. This research compares two different methods to remove the remaining error. One is a weighted covariance method, while the other

solution is to specifically model the error by adding states to the Kalman filter. This research showed that single frequency operation is sufficient for centimeter level accuracy. This means that widelane techniques are not needed. Another finding confirmed that a change in relative geometry is required to resolve the carrier-phase ambiguities. Finally, this research showed the dominant errors in a simulated pseudolite system are from residual tropospheric delay and misalignment of the pseudolites. This research lacks insights into real problems that may occur with actual measurements.

1.7.4 Naval Height Constraining. Height constraining is very applicable in naval position estimation as the height of a body of water is often well known. [27].

1.7.4.1 Improvement of Ambiguity Resolution with Constraints. In this research, [27], decreasing the time it takes to resolve ambiguities on the fly onboard a ship with two roving receivers was investigated. Several constraints were used in an attempt to aid the ambiguity resolution process. A height constraint was used as well as a heading and pitch constraint, a fixed baseline between the rover pair, and an ambiguity constraint. A pseudo-measurement was used to incorporate the known height. The height constraint was found to be the most beneficial of the constraints used in reducing the resolution time by nearly half. It was also found that the reliability of the system was increased from 80 to 95 percent.

1.7.4.2 Navigation in Constricted Waterways. Constricted waterways demand precise positions for safe navigation. This is difficult given that many times the line-of-sight GPS signals are blocked by obstructions. Two research techniques are described below to improve navigation in this environment. Both researchers include a height constraint incorporated as a pseudo-measurement.

Research by [17] involves augmenting GPS with pseudolites to give more accuracy and robustness in cases when GPS is masked by obstructions. It was found that using even a single pseudolite the HDOP is decreased dramatically as well as the worst-case horizontal error.

Augmenting GPS with GLONASS and a height constraint is a second method of improving the accuracy and robustness. Using the second constellation of positioning satellites results in an increased number of visible transmitters at any given time. The addition of a height constraint makes a further improvement to the reliability, since the height is usually known for marine applications [23].

1.7.5 LocataLite Test Examples. LocataLites have been used in several experimental trials as pilot studies of the system.

1.7.5.1 BlueScope Steel. In this pilot study, [2], the Locata system is shown to give centimeter level relative positioning precision in a severe multipath environment. The BlueScope steelworks at Port Kembla in Australia uses a large crane to move slabs of steel. The position of the crane must be tracked to assure accurate placement and inventory inside a large warehouse. Due to the metallic structure the environment is highly conducive to extreme multipath. Nevertheless, the Locata system was able to give sub-centimeter accurate positioning of the crane compared to a total station. Multipath was mitigated by careful placement of LocataLites and Locata receivers. Future testing will also give the steelworks the ability to track vehicles and steel slabs moving from outdoors to indoor environments.

1.7.5.2 Structural Deformation. In another study, LocataLites were used to measure the structural deformation of a suspension bridge [3]. The test occurred at the suspension footbridge at Parsley Bay at Sydney Harbor, Australia. Accurate measuring of bridge deformation can be difficult to attain with GPS systems, since their accuracy can fluctuate significantly depending on satellite geometry and availability. A Locata receiver was placed on the bridge with four LocataLites placed at lower altitudes. The system was initialized by manually surveying without the use of GPS. It was shown that LocataLites gave sub-centimeter level relative positioning accuracy without the use of GPS signals.

1.8 Thesis Overview

Chapter 2 presents all the pertinent background theory needed in this research. The least squares estimation methods, GPS fundamentals, and pseudolite characteristics will be discussed in-depth. Chapter 3 details the methods developed in this research for aiding the navigation solution, detecting cycle-slips, and creating simulations. Chapter 4 analyzes the results of the simulations and the processing of the real data, as well as compare the different methods with one another. Chapter 5 summarizes the results and also provides recommendations for future research in boosting the accuracy of the different methods for aiding the position solution of a pseudolite-based reference system.

II. Background

2.1 Overview

First, the GPS signal structure and measurements, which are similar to paseudolite measurements, will be discussed. The next sections will introduce least squares estimation methods. These will form the basis of the methods developed in later solution algorithms. After discussing least squares estimation, pseudolites are introduced, and they are compared and contrasted with GPS. The errors and issues that corresponds to pseudolites are then detailed. Finally, a short introduction to the specific pseudolites, from Locata Corporation, is made.

2.2 GPS Signals

In-depth presentation of GPS signals can be found in [16,19]. GPS signals operate fundamentally on two frequencies. These two center frequencies are 1575.42 Mhz and 1227.6 Mhz, termed L1 and L2 respectively. The L1 channel transmits three messages, a coarse-acquisition (C/A) code, a precise (P) code, and a navigation message. L2 only contains the P code and the navigation message. The signals are transmitted on the carrier frequency using a bi-phase shift key (BPSK) modulation. The GPS satellites have very expensive clocks onboard that guarantee the signals are transmitted at synchronized and precise times. With knowledge of the satellite's location, given through ephemeris data in the navigation message, and knowledge of the signal structure, a receiver can track a satellite's signal and knowing the transmission time can create a pseudorange measurement. This measurement is not the true range to the satellite due to the effects of clock errors. Another measurement that is available to the receiver is a carrier-phase measurement. A receiver tracks the carrier signals phase component and can determine a very accurate measure of distance to the satellite as long as the number of complete signal cycles that occurred before reception is discovered. The phase can be measured very accurately, which can be converted to a distance using the wavelength of the signal. Thus, with a wavelength of 19.03 cm

using the L1 signal and 24.42 cm using the L2 signal, a carrier-phase measurement can be accurate to within centimeters by measuring phase within 1/20th of a cycle.

Pseudolite signals are designed very similar to GPS. Similar methods for attaining pseudorange and carrier-phase measurements are used. A third measurement that will be exploited is the signal power measurement. The signal-to-noise ratio (SNR) will be measured at the receiver to give indications of poor or bad measurements.

2.2.1 Pseudorange Measurements. Pseudorange, commonly called code, measurements can be expressed as:

$$\rho = r + c(\delta t_u - \delta t_{sv}) + T + I + m_\rho + v_\rho \tag{2.1}$$

where

ρ = pseudorange measurement (meters)
r = true range between receiver and transmitter (meters)
c = speed of light (meters / second)
δt_u = receiver clock error (seconds)
δt_{sv} = transmitter clock error (seconds)
T = errors due to troposphere (meters)
I = errors due to ionosphere (meters)
m_ρ = errors due to pseudorange multipath (meters)
v_ρ = pseudorange errors due to receiver noise (meters)

The time errors that are associated with this measurement come directly from the errors in the clocks in the receiver and the transmitter. For GPS, the transmitter clock error is very small, since atomic clocks are being used. The receiver clock is usually not an atomic clock, and thus contains large errors. This receiver clock error must either be estimated or eliminated through differencing.

Nearly the same measurement model is used with pseudolites, except for the ionospheric error term. Since pseudolites are generally ground based, they do not

travel through the ionosphere, and thus do not contain ionospheric errors. It is important to note that with pseudolites the transmitter clocks will not be atomic based, and therefore the transmitter clock error may be much larger than with GPS. As will be seen later, the pseudolite used in this research handles the problem of transmitter clock error in a unique way.

2.2.2 Carrier-Phase Measurements. Carrier-phase measurements are similar to code measurements, but they can be much more accurate since the phase of a signal can be measured with very high accuracy. This measurement can be expressed as

$$\phi = \lambda^{-1}(r + c(\delta t_u - \delta t_{pl}) + T - I + m_\phi + v_\phi) + N \tag{2.2}$$

where

ϕ = Carrier-phase measurement (cycles)
λ = carrier wavelength (meters / cycle)
r = true range between receiver and transmitter (meters)
c = speed of light (meters/second)
δt_u = receiver clock error (seconds)
δt_{pl} = transmiter clock error (seconds)
T = errors due to troposphere (meters)
I = errors due to ionosphere (meters)
m_ϕ = errors due to carrier-phase multipath (meters)
v_ϕ = carrier-phase errors due to receiver noise (meters)
N = carrier-phase integer ambiguity (cycles)

Note that the sign of the ionospheric error is reversed from the code case. This occurs because the phase of the carrier is advanced in the ionosphere instead of delayed, as occurs in the pseudorange. This creates the problem of code-carrier divergence in the presence of large ionospheric error. Again the ionospheric delay is neglected when using the above measurements with pseudolites.

The carrier-phase ambiguity term is unknown and must be resolved before an accurate solution is obtained. This process is called "ambiguity resolution," and it is described in the next section.

2.2.3 Carrier-Phase Ambiguity Resolution. When using carrier-phase measurements, the integer ambiguity term must be resolved to achieve accurate positioning. The integer ambiguity represents the unknown number of cycles that are present before integration of the Doppler measurement begins. The ambiguities are constant for the measurement history as long as the measurements are continuous and free of cycle slips. Solving for the ambiguities usually requires enough angular motion between the reference system and the mobile receiver for the correct ambiguities to become apparent. In GPS, this can take tens of minutes since the angular motion between a ground based mobile receiver and the satellite constellation is slow. In a pseudolite system, the angular motion can be much more active and the time required for resolution of the ambiguity may be much shorter.

The ambiguity is in reality an integer, since it represents a measure of whole cycles. It is difficult to force an algorithm to estimate the ambiguity state as an integer. This is doubly difficult since any errors that are bias like in the system can be indistinguishable from being part of the ambiguity. This gives rise to a method of fixing the ambiguities to integers after they have been estimated as floating values.

There are many ways that the integer ambiguity is found, many rely on the use of Kalman filter estimates of the ambiguities and the covariances. Examples of this are the Least squares AMbiguity Decorrelation Algorithm (LAMBDA) and the Fast Ambiguity Search Filter (FASF). Both methods are described in [20].

In this research the ambiguities will remain floating. This means that integer ambiguity resolution will not be done. In the current stage of development, the Locata system outputs phase measurements that have non-integer ambiguities.

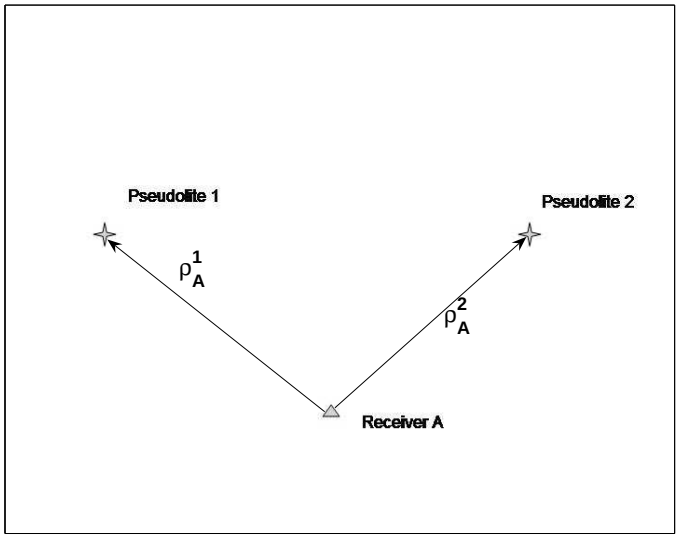

Figure 2.1: Single Difference Between Receiver A and Pseudolites 1 and 2

2.2.4 Single Differencing. Single differencing is used to eliminate or reduce some errors in measurements. When linear combinations of measurements between receivers, transmitters, or times are taken the common errors can be removed. Single differencing between two transmitters (pseudolites) will use the notation (∇).

Figure 2.1 shows how single differencing between two pseudolites would appear. Single differencing with code measurements as in Figure 2.1 is defined as

$$\nabla\rho_A^{12} = \rho_A^1 - \rho_A^2 \tag{2.3}$$

where ρ_A^1 is the code measurement between receiver A and pseudolite 1, and ρ_A^2 is the code measurement between receiver A and pseudolite 2.

Single differencing will eliminate the receiver clock error and reduces the tropospheric errors. This can be seen by combining Equations (2.1) and (2.3) to yield

$$\begin{aligned}\nabla\rho_A^{12} = r_A^1 + c(\delta t_{u_A}^1 - \delta t_{pl}^1) + T_A^1 + m_{\rho_A}^1 + v_{\rho_A}^1 \\ -r_A^2 - c(\delta t_{u_A}^2 - \delta t_{pl}^2) - T_A^2 - m_{\rho_A}^2 - v_{\rho_A}^2\end{aligned} \tag{2.4}$$

Combining like terms gives

$$\begin{aligned}\nabla\rho_A^{12} = (r_A^1 - r_A^2) + c(\delta t_{u_A}^1 - \delta t_{u_A}^2) - c(\delta t_{pl}^1 - \delta t_{pl}^2) \\ +(T_A^1 - T_A^2) + (m_{\rho_A}^1 - m_{\rho_A}^2) + (v_{\rho_A}^1 - v_{\rho_A}^2)\end{aligned} \tag{2.5}$$

The receiver clock errors $\delta t_{u_A}^1$ and $\delta t_{u_A}^2$ are the same for receiver A so they will cancel. The remaining differences will be represented as (∇). Equation (2.5) can now be rewritten as

$$\nabla\rho_A^{12} = \nabla r_A^{12} + c\nabla\delta t_{pl}^{12} + \nabla T_A^{12} + \nabla m_{\rho_A}^{12} + \nabla v_{\rho_A}^{12} \tag{2.6}$$

In the GPS case, the differencing will reduce the tropospheric error, but will increase the multipath and measurement noise by a factor of $\sqrt{2}$.

Single differencing with carrier-phase measurements is very similar to the above code differencing and yields

$$\nabla\phi_A^{12} = \lambda^{-1}(\nabla r_A^{12} + c\nabla\delta t_{pl}^{12} + \nabla T_A^{12} + \nabla m_{\phi_A}^{12} + \nabla v_{\phi_A}^{12}) + \nabla N_A^{12} \tag{2.7}$$

The receiver clock error has again dropped out, and the differenced integer ambiguity term has appeared. Examples of double differencing are shown in [8, 16, 19, 20]. This technique is used to eliminate both receiver and pseudolite clock errors. It also allows further reduction of the atmospheric errors, but with a penalty of further increased multipath and measurement noise.

2.3 Least Squares Estimation

Least squares estimation is a very useful and common tool in estimation. Examples and similar derivations can be found in [7, 16]. Given measurements of some system, it is possible to find the characteristics of that system. The characteristics of the system are termed the system states. They must be related to the measurements in some known way. Suppose there is a linear relationship:

$$\mathbf{z} = \mathbf{H}\mathbf{x} + \mathbf{v}, \tag{2.8}$$

where $\mathbf{z}$ is the m-dimensional measurement vector, $\mathbf{H}$ is the $m \times n$ measurement matrix, $\mathbf{v}$ is a vector of m unknown errors, and $\mathbf{x}$ is the n-dimensional unknown state vector. If the number of measurements, m, is greater than the number of states, n, the system is over-determined. This is the common case in this research. If m where to be less than n, the system would be under-determined, and no solution would be found. For a solution to be determined, $\mathbf{H}$ must also have a rank of n. If this is not the case, then there is a problem with unobservability, which will be discussed later. The goal is to find the best estimate of the states, $\hat{\mathbf{x}}$, given the measurements.

The LSE method attempts to minimize the difference in a least-squares sense between the measurements and an estimate of the measurements based upon estimates of the unknown states, $\mathbf{x}$ and the known matrix $\mathbf{H}$. The least squares scaler error is written as

$$J = (\mathbf{z} - \mathbf{H}\mathbf{x})^T (\mathbf{z} - \mathbf{H}\mathbf{x}) \tag{2.9}$$

The estimate of the vector $\mathbf{x}$ is found by minimizing the scalar error with respect to the state vector $\mathbf{x}$. This is done by setting the derivative of J with respect to (wrt) $\mathbf{x}$ to zero, and solving for $\mathbf{x}$. Once this is done, the solution for $\hat{\mathbf{x}}$ comes forth as

$$\hat{\mathbf{x}} = \left(\mathbf{H}^T\mathbf{H}\right)^{-1} \mathbf{H}^T\mathbf{z} \tag{2.10}$$

If $\mathbf{H}$ is not of full rank then the inverse of $\mathbf{H}^T\mathbf{H}$ is singular. Problems also occur if $\left(\mathbf{H}^T\mathbf{H}\right)^{-1}$ is nearly singular, which is the case with poor observability. In the observable case, the least squares estimate of the states is obtained.

2.3.1 Weighted LSE. When trying to estimate the states of a system it is important to use all the information possible. When considering measurements it is important to incorporate the knowledge of the measurement errors. Given Equation (2.8), the measurement error vector can be assumed to be zero-mean white Gaussian noise with covariance matrix $\mathbf{R}$, where

$$\mathbf{R} = E\{\mathbf{v}\mathbf{v}^T\} \tag{2.11}$$

The measremtent noise covariance matrix will effectively represent the errors that are expected in the measurements and also any correlation of errors between the different measurements.

The noise covariance matrix is applied in least squares estimation and forms the method commonly called weighted least squares (WLS). A slight change occurs in the LSE algorithm and now appears as

$$\hat{\mathbf{x}} = \left(\mathbf{H}^T\mathbf{R}^{-1}\mathbf{H}\right)^{-1}\mathbf{H}^T\mathbf{R}^{-1}\mathbf{z} \tag{2.12}$$

As will be seen later, different measurements with different noise variances will get weighted differently in the WLS structure. This will allow more accurate measurements to have more influence on the estimate.

2.4 Non-Linear Least Squares Estimaion

Previously, the relationship between the states and the measurements was assumed to be linear. In many situations this is not a valid assumption. Instead of having a direct linear relationship, the measurements will be a nonlinear representation of the system states. This is represented below.

$$\mathbf{z} = h(\mathbf{x}) + \mathbf{v} \tag{2.13}$$

Since $h(\mathbf{x})$ is potentially nonlinear, the previous method of least squares estimation cannot be used. The iterative least squares (ILS) will be used. This method starts with an initial estimate of the states $\hat{\mathbf{x}}_o$ and uses the measurements to calculate a corrected state estimate $\hat{\mathbf{x}}_c$. The corrected state estimate then becomes the current state estimate $\hat{\mathbf{x}}$, which replaces the initial estimate. This process is repeated until there is convergence. Convergence of the solution is tested before the estimate is validated. Convergence of the solution can depend on several factors such as accuracy of the initial estimate and observability of the states. Details of this process are described below.

2.4.1 Iterative Least Squares. The iterative estimation method involves correcting the estimates of the states at each iteration. To update the current state estimate and create the corrected state estimate, the following relationship is defined.

$$\hat{\mathbf{x}}_c = \hat{\mathbf{x}} + \widehat{\Delta\mathbf{x}} \tag{2.14}$$

where $\widehat{\Delta\mathbf{x}}$ is defined as the estimated error in the state estimate.

The measurement residuals are the difference between the actual measurement vector $\mathbf{z}$, and the modeled measurements given the current state estimate $\hat{\mathbf{x}}$.

$$\Delta\mathbf{z} = \mathbf{z} - h(\hat{\mathbf{x}}) \tag{2.15}$$

The measurement residual vector $\Delta\mathbf{z}$ can also be represented using the state correction $\Delta\mathbf{x}$. A first-order expansion is used to relate the measurement residual to the error in the state estimate as follows:

$$\Delta\mathbf{z} = \mathbf{H}\Delta\mathbf{x} + \mathbf{v}, \tag{2.16}$$

where $\Delta\mathbf{x}$ is the error in the state estimate. The sensitivity matrix $\mathbf{H}$ is the same as above and embodies the relationship of the states and measurements. Now the relationship is non-linear, and $\mathbf{H}$ is the matrix of partial derivatives evaluated from the current state estimate.

$$\mathbf{H} = \left.\frac{\partial h}{\partial \mathbf{x}}\right|_{\hat{\mathbf{x}}} \tag{2.17}$$

The ith row of $\mathbf{H}$ is made up of the partial derivatives of the ith entry in the h vector wrt the states $\mathbf{x}$. Therefore, $\mathbf{H}$ is an m by n matrix, with m remaining the number of measurements and n the number of states.

Since second-order terms have been ignored, the previous development with a linear term to obtain Equation (2.10) can be followed to similarly obtain the following,

$$\widehat{\Delta\mathbf{x}} = \left(\mathbf{H}^T\mathbf{R}^{-1}\mathbf{H}\right)^{-1}\mathbf{H}^T\mathbf{R}^{-1}\Delta\mathbf{z} \tag{2.18}$$

It is important to note that during each iteration the $\mathbf{H}$ matrix must be re-evaluated at the current state estimate. Each iteration will use the corrected state estimate from the previous iteration to linearize h and form $\mathbf{H}$.

As stated, this process of correcting the state estimate is repeated until sufficient convergence is obtained. Convergence is indicated by the change in the state estimate ($\widehat{\Delta\mathbf{x}}$) becoming sufficiently small. A threshold can be set that is based upon knowledge of the system and measurements. Using a sum of squares of $\widehat{\Delta\mathbf{x}}$, the solution is either declared valid or another iteration is begun. In this manner the non-linear state estimate is obtained. The accuracy of the above linearization is dependent on assuming the second-order effects of the states in the system are minimal.

2.5 Batch Least-Squares

The above methods of Least-Squares Estimation are commonly used in an epoch by epoch process. This means that the state vector and measurements for each time

epoch are used independently from previous and subsequent times. The states at a given epoch are estimated using the measurements pertaining to that time before another LSE process is started for the next epoch. This is common to the techniques used in Kalman Filter applications.

This method ignores the common elements between epochs. A batch process considers all the states and measurements together. The states are not constrained to be related to any single epoch. Everything is estimated simultaneously. This allows, for example, the ambiguity states that are common to many epochs, to be estimated properly.

Estimating all the states using all the measurements can involve much larger matrices than normally encountered. This will motivate some ad hoc techniques to minimize the size discussed in the previous chapter.

The batch ILS method will allow other errors that are only observable through geometry changes as well. Errors such as residual tropospheric delay and transmitter position error are future avenues of research that are expected to see benefit using batch ILS estimation.

2.6 Pseudolites

Pseudolites, standing for pseudo-satellites, are usually ground-based transmitters that propagate GPS-like signals. Pseudolites have been used to augment GPS for many years [10, 26]. One reason for pseudolite augmentation of GPS is to boost the availability of GPS by adding ground based signals that are copies of the GPS signal. This allows locations with poor satellite visibility to achieve position solutions. Pseudolites are much cheaper than satellites and are much more easily customized. Different algorithms and signal types can be used to mitigate different types of error. A thorough discussion of pseudolites can be found in the following references [10, 26].

Many of the errors in the pseudolite measurements are similar to the errors in the GPS measurements. Tropospheric error, multipath, receiver noise, etc. are all

similar. Other pseudolite implementation issues are synchronization and the near/far problem. Ionospheric error will be completely neglected, since the signals will not be propagating through the ionosphere. These error sources will be discussed briefly, and the techniques to mitigate them will be discussed after the measurements themselves are introduced.

2.6.1 GPS vs Pseudolites. The core difference between GPS and pseudolites lie in the location of the transmitters. GPS transmitters are located on satellites 20,000 km in the sky. Pseudolites can be placed on the ground in almost any location. The following are a list of many differences between GPS and pseudolites.

- Pseudolites can operate on frequencies other than the L1 and L2 frequencies associated with GPS. This is key for the purposes of this research, since the system will be used in the presence of jamming on these two frequencies.
- Pseudolite signals are based on the ground and therefore do not pass through the ionosphere as GPS signals do. Therefore the usual ionospheric errors are not present.
- Angular motion between a mobile receiver in motion and the transmitters is greater in pseudolite systems then with GPS. This maybe related to how quickly carrier-phase ambiguities are resolved.
- Multipath in a psedolite system can be much more severe. The elevation angles of the transmitters can be much lower than experienced in GPS. With much smaller glance angles there is much more position correlated multipath.
- While signal strength with pseudolites can be much more powerful than with GPS, the power at the receiver has the potential to be highly dynamic. This can cause problems in receiver design.
- Instead of orbital erros in GPS, pseudolite systems are very sensitive to accurate surveying of transmitter position errors. The physical position of the transmitter and the phase center of the antenna must be found accurately.

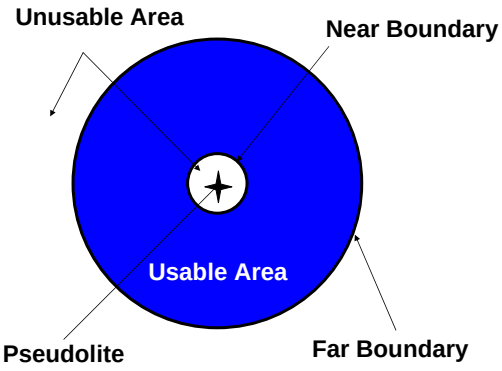

Figure 2.2: Illustration of Near/Far Problem

2.6.2 Pseudolite Errors. The following sections provide further discussion of errors that occur with the use of pseudolites and the methods used to mitigate these errors.

2.6.2.1 Near-Far Problem. The near/far problem is an issue for both pseudolite augmented GPS systems and for pseudolite only based systems. Maximizing the transmitters' useful distance requires increase in the transmission levels. The problem occurs as a receiver approaches a pseudolite, the signal from that pseudolite drowns out the signals from the other pseudolites, making it impossible to have a solution. Figure 2.2 shows the donut region that is the usable area around a pseudolite. A higher quality pseudolite will have a larger usable region.

The near/far problem can be ignored in some applications if the usable area is acceptable, but this is not typically the case. The standard method to solve this problem is to use a pulsed signal scheme. In this type of system, each pseudolite will

transmit on a predefined duty cycle. This allows a receiver to track other desired signals while in close proximity to a given pseudolite. This has been used with GPS augmentation for landing systems in the past. The problem of synchronization now becomes tied to the near/far problem, because each individual pseudolites must be synchronized so that it is pulsing at the correct time relative to the other pseudolites. The pulsing scheme is commonly referred to as Time Division Multiple Access (TDMA). Other forms of signal separation that can be adopted from the communications industry are Frequency Division Multiple Access (FDMA) and Code Division Multiple Access (CDMA). More detailed discussion of these schemes are found in [10].

2.6.2.2 Synchronization. Synchronization of the signals is vital to reference systems. In GPS, the satellites use extremely accurate atomic clocks. These clocks are very expensive and not feasible for pseudolites. The signals must be synchronized so that the user can determine what time it was transmitted. This is the only way the user can determine his pseudorange to the pseudolite. In many cases when pseudolites where used to augment GPS, the pseudolites are all synchronized to GPS time from the satellite signals themselves. This required the availability of GPS at the location of each pseudolite. GPS will be unavailable in this test, and the pseudolites must be synchronized using a different method.

To overcome this problem a new technology has been developed by a company called Locata, whereby each pseudolite has the ability to precisely synchronize with other pseudolites in the system. This feature and others will be discussed later in Section 2.7.

2.6.2.3 Tropospheric Error. A large source of errors in the measurements is due to the troposphere. The troposphere is the portion of the atmosphere that is neutral, roughly 0-10km in altitude [25]. In the proposed system, the signals will be propagating completely in the troposphere. The delay experienced by the signals depend on the refractivity index of the air mass the signal is travelling through. This index is a function of the density of the air, which is in turn due to the density

of the dry and wet components of the air [16]. Roughly 90% of the delay is due to the dry portion of the density. For GPS signals, this portion can be predicted to within 1% @ zenith (90 degree elevation). The remaining 10% due to the water vapor is much harder to calculate and is only predictable to 10-20% at zenith [19]. For pseudolite applications, the errors are amplified. A commonly used model with GPS is the Hopfield model. It is based on predicting the refractivity index at an altitude based on the refractivity at the surface. The tropospheric error is usually calculated at zenith and then transformed to the desired elevation using a mapping function. These methods can be inadequate for pseudolite applications, because the mapping functions become inaccurate at lower elevations, which occur regularly for ground-based pseudolites. More applicable models must be introduced for use in pseudolite applications.

The tropospheric model to be used can be found in [8, 9, 11]. It is a function of temperature, atmospheric pressure, relative humidity, elevation angle, and range. The atmospheric parameters are measured at a ground based reference station. The delay for the mobile receiver is defined as

$$\begin{aligned}
\tau_{APL,u}(R_u, \Delta h_u) &= \frac{\Delta\tau_{v,dry} + \Delta\tau_{v,wet}}{\sin(el_u)} = \frac{(\Delta\tau_{v,dry} + \Delta\tau_{v,wet})}{\Delta h_u} R_u \\
&= \frac{77.6 P_s \times (42700 - h_s) \times 10^{-6}}{5 T_s \Delta h_u} \left[\left(1 - \frac{\Delta h_{APL}}{42700 - h_s}\right)^5 - \left(1 - \frac{\Delta h_{APL} + \Delta h_u}{42700 - h_s}\right)^5 \right] R_u \\
&\quad + \frac{N_s \times (13000 - h_s) \times 10^{-6}}{5 \Delta h_u} \left[\left(1 - \frac{\Delta h_{APL}}{13000 - h_s}\right)^5 - \left(1 - \frac{\Delta h_{APL} + \Delta h_u}{13000 - h_s}\right)^5 \right] R_u
\end{aligned} \tag{2.19}$$

where the variables are defined as

$\tau_{APL,u}$ = tropospheric delay for mobile receiver (meters)

R_u = slant range between the pseudolite and user (meters)

Δh_u = the height of the user above the pseudolite (meters)

$\Delta\tau_{v,dry}$ = differential vertical dry delay (meters)

$\Delta\tau_{v,wet}$ = differential vertical wet delay (meters)

el_u = elevation angle in radians

Δh_{APL} = difference in height between pseudolites and reference receiver

h_s = height of reference receiver

P_s = surface pressure (millibars)

T_s = surface temperature (Kelvins)

N_s = surface refractivity

The tropospheric equation is valid for all elevation angles except zero. A modified equation for this indeterminate case can be found in [11].

After the majority of the tropospheric error is eliminated through use of the model and reduced by single differencing, the remaining error is termed the residual tropospheric error. Although this is still very small, it cannot be ignored when seeking centimeter level accuracy. This residual error can be modelled as a scale factor and reduced or incorporated as a state to be estimated. These methods are part of the research in this thesis and are discussed later in this paper. Additional details can be found in [8, 9].

2.6.2.4 Multipath Error. Multipath error in a pseudolite-based reference system is similar to using GPS. The source of the error is still the same. Signals from the sending antenna travel a true path to the receiving antenna, but they can also be reflected off the surrounding landscape to the receiving antenna. The error is caused by these reflections travelling multiple reception paths. In pseudolites, this error is often amplified. The problem is increased with the low glance angles sometimes associated with pseudolite locations. A more complex problem lies in the use of differential techniques and synchronizatiion with pseudolites.

In GPS applications the satellites are moving and a stationary receiver will not have a biased multipath since the source of the signal is moving throughout the sky. In a pseudolite system the transmitters do not move relative to each other. This can create a standing multipath dilemma between pseudolites. In a differential pseudolite system the standing multipath is found between the reference receiver and the pseudolites. In the test designed for this research, the pseudolites use a synchronization scheme requiring the pseudolites to receive signals from each other. This leads to a standing multipath problem.

Multipath error can be difficult to eliminate. In GPS applications, special antennas can be used to reduce most multipath errors. This is easier with satellite applications, since most usable signals are all above 15 degrees. In pseudolite applications, signals are coming from ground based transmitters and force different receiver antennas.

2.6.2.5 Geometry/Observability. In GPS, geometry plays a large role in the accuracy of the solution. Poor geometry can easily be the largest source of error. Many times, waiting for better satellite geometry is the only solution. This is one of the reasons that GPS is sometimes augmented with pseudolites. Having satellites only low on the horizons results in a larger error in the vertical direction. This is due to the poor observability in that direction by the measurements. The same problem occurs with pseudolites.

In a landing scenario with ground based pseudolites, at the moment of landing the receiver and all the pseudolites are very close to being in the same plane. As they come closer to lying in the same plane, the ability of the system to determine the vertical position deteriorates. This could be solved similarly to the case with GPS, except instead of waiting for a satellite to move into a better position, the pseudolites can be placed in a better geometry or more pseudolites can be added to the existing setup to create a better geometry. Both approaches have the same problem though. To achieve better observability in the vertical direction, some of the

pseudolites must be placed such that there is a significant elevation angle between it and the receiver (in order to make the measurement geometry non-coplanar). This can be very problematic at an airfield, where tall objects and landscapes have been avoided for safety concerns. Additionally, placing pseudolites on towers maybe undesirable, due to the swaying of the towers. This will cause a very significant change in the location of the transmitter and will introduce an unacceptable error, when centimeter accuracy is needed.

Even in GPS cases geometry/observability becomes a problem. In naval navigation there can be cases of obstructed views of satellites. With poor visibility the observability of the vertical dimension can be poor. In many naval cases the height of the water level, thus the receiver height, is well known, and can be incorporated as a constraint in the solution [17, 23, 27]. Such a height constraint can be implemented by using a pseudo-measurement of the height.

2.6.2.6 Receiver Noise. Receivers not only measure the desired signals, but also introduce unwanted random noise. This error is caused by many sources. and is dependent upon receiver design and location. The receiver measurements are affected by RF radiation in the band of interest; the antenna, amplifiers, cables, and the receiver; multi-access noise (i.e., interference from other GPS signals and GPS-like broadcasts from system augmentations); and signal quantization noise [16]. Receiver noise error is not a bias and can be mitigated by filtering.

2.7 LocataLites

The pseudolites that will be used for this research are from Locata Corporation [1, 4–6]. These pseudolites, termed LocataLites, are a novel design that solves some of the problems discussed in the previous sections. LocataLites can be used to set up a LocataNet, which is a network of synchronized LocataLites, and has potential for near-centimeter-level accuracy using carrier-phase positioning. These pseudolites solve the problem of synchronization with a method called TimeLoc. TimeLoc syn-

chronizes LocataLites, and can be described in a series of steps [4].

1. LocataLite A transmits a C/A code and carrier signal on a particular PRN code.
2. The receiver section of LocataLite B acquires, tracks and measures the signal (C/A code and carrier-phase measurements) generated by LocataLite A.
3. LocataLite B generates its own C/A code and carrier signal on a different PRN code to A.
4. LocataLite B calculates the difference between the code and carrier of the received signal and its own locally generated signal. Ignoring propagation errors, the differences between the two signals are due to the differences in the clocks between the two devices, and the geometric separation between them.
5. LocataLite B adjusts its local oscillator using Direct Digital Synthesis (DDS) technology to bring the code and carrier differences between itself and LocataLite A to zero. The code and carrier differences between LocataLite A and B are continually monitored so that they remain zero. In other words, the local oscillator of B follows precisely that of A.
6. The final stage is to correct for the geometrical offset between LocataLite A and B, using the known coordinates of the LocataLites, and after this TimeLoc is achieved.

This method of synchronization can be replicated with many LocataLites creating a network of synchronized pseudolites without the use of expensive atomic clocks.

III. Algorithm Development

3.1 Overview

This chapter will describe the algorithms developed for aiding a pseudolite reference system with height determination. Since a non-linear, iterative, batch least squares estimation method forms the basis of each algorithm, the initial setup for each algorithm is very similar, and will be discussed first. Following the initial setup, the surface grid information will be introduced. An important aspect of height determination methods in this research involves the pre-defined surface created from GPS surveys. Finally, the algorithms that were developed will be introduced next. Each method will be covered, and important characteristics of each will be illustrated.

3.2 Initial Algorithm Setup

3.2.1 Carrier Phase Ambiguities. For precise positioning, it is mandatory that carrier-phase measurements be used. As discussed, this means that the related ambiguities must be determined. A batch least squares technique is used in this research for this purpose.

The ambiguities are found through geometry change. Having a large time history of measurements without any motion will result in little/no observability into the ambiguity states. Along the same lines, there is little gain in having a time history of 1000 epochs over that of 10 epochs if there is the same amount of geometry change. This motivates the idea of pruning the epochs that will be used in the ambiguity search process. Creating a batch process with an over-abundance of measurements that will not gain any more useful information only impedes the solution process. The ILS solution contains an n by n matrix inversion, where n is the number of states. Each epoch used in the solution adds 2 or 3 states, depending on the solution type, to the overall state vector. This inversion can quickly become a computational problem for a processor. Allowing the algorithms to only select out a predefined number of epochs spanning the time that an ambiguity is present, captures all the needed geometry change that is available and minimizes the number of states. After these

ambiguity states are found, an epoch by epoch ILS position solution can be run with the known ambiguities no longer being estimated. This final solution method has no need to be a batch process and is very straightforward.

One major problem still exist. Using the batch process, each ambiguity state is tied to the measurements at each epoch. Any time there is a cycle slip, the ambiguity can change. From that time forward the ambiguity state before the slip is no longer associated with any new measurements. This requires that cycle slips be identified. If a cycle slip goes undetected, the ambiguity estimate that is attained will be completely invalid, and will cause large errors in the position solution.

3.2.1.1 Epoch Selection. Assuming cycle slip detection has been done (which is discussed in the following section), the complete set of ambiguities and the epochs and measurements they are associated with are known. The true epochs that will be used in the batch ILS process must be selected. The goal of the batch process is to find the floating point ambiguities, so it must select the epochs that span the lifetime of all the ambiguities. Each transmitter, and its related carrier-phase measurements, will have a predetermined number of ambiguity states. Selecting a given number of epochs evenly spaced over the life of each ambiguity should maximize the observability of the ambiguities for that specific transmitter. This approach is taken for each transmitter. Since the number of ambiguities and their individual time periods of validity do not necessarily coincide between transmitters, it is necessary to include all the needed epochs for each transmitter. This results in some epochs that are duplicated and some that are very close together. Some epochs can be eliminated to keep the size of the batch process small. Duplicated times can first be eliminated, and then times that are close together can be combined by merging them together and using an epoch between the two. This will maintain the needed epochs for estimation of the ambiguities, while creating a smaller number of measurements and states for a manageable batch process.

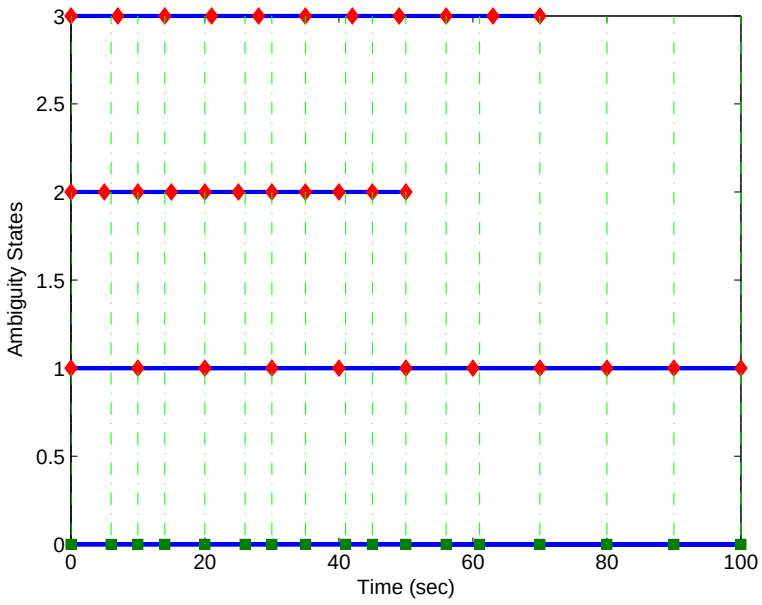

Figure 3.1: Example of epoch selection for batch processing. There are three ambiguities shown that span different times. Each has diamonds indicating preferred epochs spaced evenly over their time of validity. Along the x-axis there are squares that represent times chosen for use in the batch process.

The epoch selection and pruning process is illustrated in Figure 3.1. Given three ambiguities that span the time history with differing validity regions, epochs must be selected that represent the ambiguities and are not repeated or too close together. Each ambiguity has initially evenly space epochs that would make ideal choices to represent that ambiguity. With multiple ambiguities it can be seen that there are repeated epochs and some epochs that are close together. Along the bottom of the figure are selected epochs that are projected vertically to show how some epoch possibilities are merged to form a single epoch choice. In this case, 17 of the 24 unique epoch possibilities are selected for the processing of the batch least squares estimation.

3.2.2 Cycle Slip Detection. Cycle slip detection is necessary when processing carrier-phase measurements. In some receiver designs an output can indicate if a cycle slip has occurred. Using the change in phase measurements between epochs,

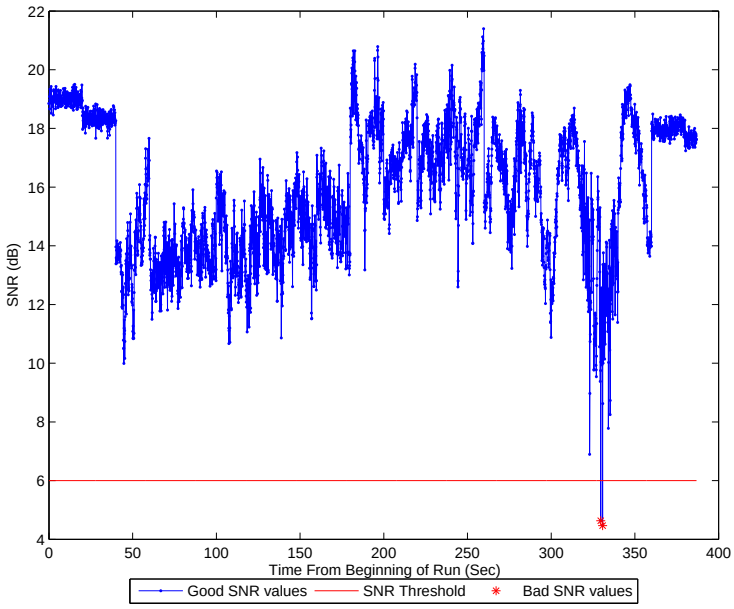

Figure 3.2: Example of a typical SNR plot shown with bad measurements indicated as being below an SNR bound. In this case there are two times that the SNR threshold is crossed.

it is possible to indicate a cycle slip from an uncommonly large change in the phase measurement itself. In GPS cases, a cycle slip happens instantaneously, making it easier to identify the erroneous event.

In its current configuration, the LocataLite can make cycle slip detection more difficult. The receiver is not able to output a cycle slip indicator, and cycle slips do not appear instantaneously as in GPS. From observation of test data, it is apparent cycle slips can occur over a gradual time. Although, the receiver remains in frequency lock with the measured signal, no effort is made to maintain the phase at zero. During a period of high multipath, this allows the phase to drift slowly and cause a drifting cycle slip instead of an instantaneous error.

In an attempt to locate the cycle slips, the SNR measurements are utilized as an indicator of a weak signal, and thus potential slips. If the SNR measurement for a given transmitter drops below a pre-determined threshold, the measurements for that transmitter are suspect. More specifically, the carrier-phase measurement is assumed

to potentially have a cycle slip. This form of detection assumes cycle slips are only found in periods of low SNR. An example of this is shown in Figure 3.2. These SNR measurements are made at the receiver and correspond with a single transmitter. This is an indication of the received power of the signal from the pseudolite. In the figure, the SNR threshold is set at 6 dB. This measurement was indicated from empirical evidence from the Locata Corporation. There are two measurements that fall below this bound. For the carrier-phase measurements from this transmitter there would be two ambiguity states. One would be associated with the measurements before the possible cycle slip and the other would be associated after this time.

An illustration of how a single transmitter can have several ambiguity states is shown in Figure 3.3. The initial ambiguity related with this transmitter is set as the first ambiguity state. After each detected cycle slip, there must be a new ambiguity state for the future carrier phase measurements from this transmitter. This can be seen as the ambiguity state changes after each time it drops to 0, which is a period of invalid measurements. The carrier-phase measurements cannot be used at these times. After each possible cycle slip, a new ambiguity must be created. This explains why an ambiguity state is never reused. It is important to remember cycle slips are only assumed to be highly possible in these regions, as indicated by low SNR values.

3.2.3 Initial Trajectories. While carrier-phase measurements will be used for precise positioning, the code measurements will not be thrown away. It is important in a batch process that an initial trajectory be used as the starting point for the ILS estimation. In a normal LSE routine, the positions are found epoch by epoch, allowing the solution for the previous epoch to be used as the initial position for the next time. In a batch process, there must be an initial guess for every epoch simultaneously. Furthermore, this initial guess must be different for at least some epochs. If a single position were used for all epochs as the initial guess, the calculation of the sensitivity matrix $\mathbf{H}$ would produce no information for determining the ambiguities. These

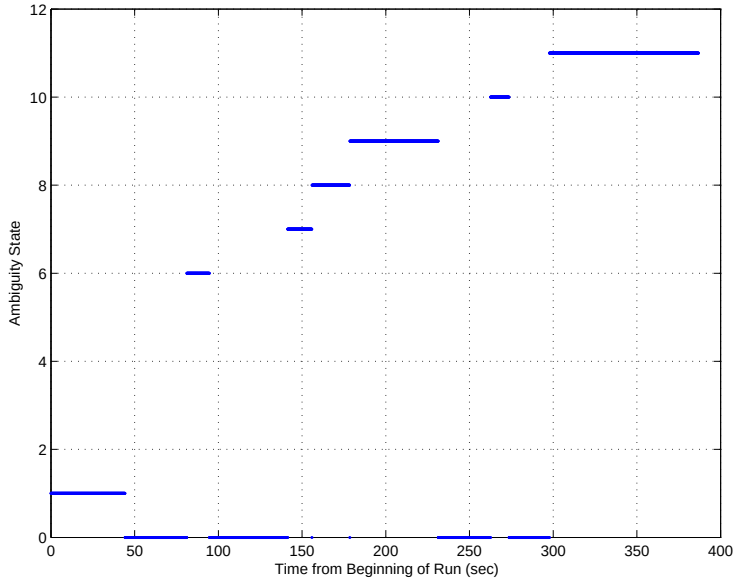

Figure 3.3: Example of the changing ambiguity states for a single transmitter. This plot shows which ambiguity state is associated with this transmitter at each epoch. An ambiguity state of 0 indicates the SNR from this transmitter is below the threshold, and a cycle slip has likely occurred.

states are dependent on geometry change, starting each epoch at the same point causes immediate divergence.

The initial trajectory that is needed for formulation of the batch process is found using the pseudorange measurements. This initial trajectory must only be accurate enough to allow the batch ILS process to converge. The pseudorange measurements are generally accurate enough for this purpose. Since single differenced measurements are being used, there is no state associated with the removed receiver clock bias. The initial positions are calculated using the same ILS process, but an epoch by epoch approach is used instead of a batch process.

3.2.4 Frame Rotations. This research will base all calculations in the East North Up (ENU) coordinate frame. Many algorithms only focus on 2-dimensional solutions. Given the ground based nature of pseudolite systems, the horizontal plane

that is tangent to the surface of the earth is the best solution plane. Confining the solution to this plane in Earth Centered Earth Fixed (ECEF) coordinates would be overly difficult. In choosing the ENU frame, the solution can be confined to the horizontal plane and elimination of the vertical direction is trivial. Conversion of the pseudolite locations from ECEF to ENU coordinates is accomplished. After an origin for the ENU frame is chosen all the locations are calculated in the new frame.

A further coordinate rotation was used for use with real data. In the real world road test conducted in relation to this research, a road was mapped and traversed using GPS receivers and a Locata receiver. The road travelled was not aligned with East or North. In later sections the creation of the GPS surveyed grid will be detailed, but creating the grid in the standard ENU frame required a large number of invalid grid points due to the nature of the road geometry. Instead of the road spanning the length of a rectangle, which is desirable for a larger number of useful grid points, the road only spanned a diagonal section of a more square grid. To facilitate a better use of computing resources, the coordinate frame was rotated by 5 degrees. This aligned the road so as to maximize the number of valid points in the grid.

Figure 3.4 illustrates this concept by providing the exact example explained above. Figure (a) shows the test road, viewed from above, in the normal ENU frame. The road track is along the diagonal of where the grid will lie. All of the empty space in the grid will be invalid points that cannot be used, but are present and increase the calculation time. Figure (b) shows the same road, also viewed from above, but this time the ENU frame has been rotated 5 degrees, so the road now fills the area where the grid will lie. This increases the number of useful grid points.

3.2.5 Measurement Formulation. Measurements from each pseudolite are logged in the receiver. Pseudoranges, carrier-phase, and SNR measurements are available. As previously discussed, single differenced measurements will be used in order to eliminate the receiver clock error. A base transmitter will be chosen that will then be differenced with the remaining transmitters. This creates a set of independent

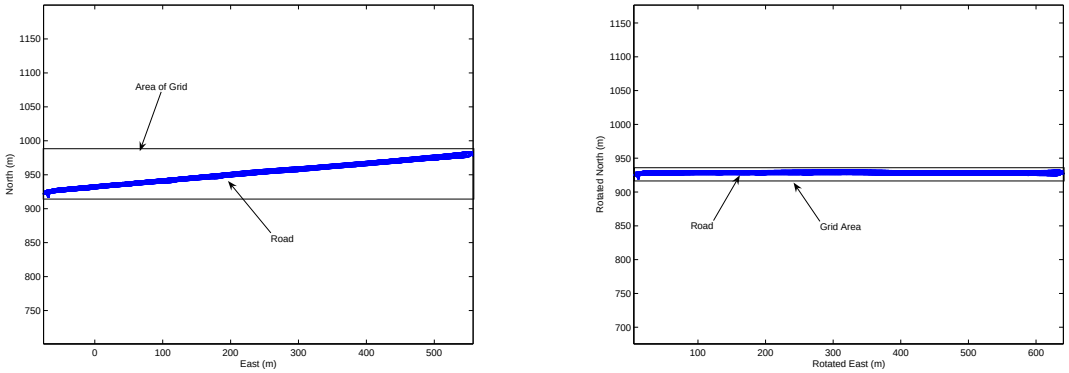

(a) (b)

Figure 3.4: (a) Horizontal view of a test road in ENU frame. Poor use of grid. (b) Horizontal view of a test road in rotated ENU frame. Road now spans grid more efficiently

combinations of the measurements. A transformation of variables can be avoided if the base transmitter is selected that has no cycle slips, otherwise it could be possible that all the single differenced measurements for an epoch could be invalidated by a cycle slip on the base measurement alone. Figure 3.5 shows a plot of all 5 transmitters and their corresponding cycle slips. Other than transmitter 4, all transmitters have at least one cycle slip. Thus number 4 is selected as the base. With 5 measurements at each epoch, there will be 4 single differenced measurements. Each will be the difference between the base and another transmitter.

3.2.6 Tropospheric Error. Although pseudolite signals do not have to deal with ionosperic error, they do deal with much more error due to tropospheric effects. It is much harder to measure the tropospheric delay close to the surface of the Earth. Many models are only valid for elevation angles greater than 15 degrees. In the test case for this research, the greatest elevation did not get above 6 degrees. A new model was used that can handle any elevation angle and relies on temperature, pressure, and relative humidity [8, 9, 11].

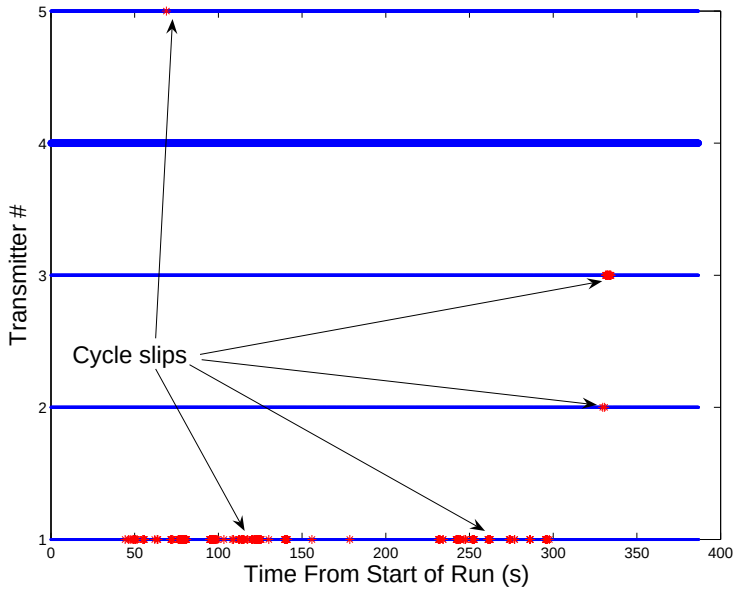

Figure 3.5: Plot of each transmitter and the cycle slips for each. Other than number 4, each transmitter experiences at least one cycle slip.

The tropospheric delay is calculated using the atmospheric parameters, pseudolite positions, and estimated receiver location. These corrections are added into the measurement residual vector, $\Delta\mathbf{z}$. In this manner the tropospheric error is modelled and mitigated.

3.3 Formation of the Surface Grid

Developing methods to use predetermined surface data to aid the height estimation is the goal of this research. For ground based applications, the test area can be surveyed using precise DGPS techniques, ensuring centimeter-level accuracy. Once this is done, a grid of the area can be created that describes the surface accurately enough to aid the least squares techniques being used. While formation of the grid is important for this research, the actual inclusion of this information into the solution is actually being investigated. Therefore little time will be spent on methods for grid creation.

In an ideal case, the surface can be surveyed in a grid fashion allowing the surveyed locations to be in a grid formation to begin with. In the road test conducted for this research, no such survey technique was possible. Instead, two GPS antennas were placed on either side of the Locata antenna. This GPS data was logged while data was collected for the pseudolite system. This not only allowed a surveyed map of points to be made of the road, but also allowed a truth trajectory to be made from the average of the two GPS solutions. Again, differential GPS methods have been applied to gain centimeter level accuracy. This required the use of a stationary GPS reference receiver as well.

3.4 Determination of a Height Using the Surface Grid

Many of the algorithms developed rely on determining the height of a horizontal position using the surface topography. Since the surface information is contained in a grid of points, interpolation of the grid must be done to find the height at some location between grid points.

Bilinear interpolation was used to find the height of a horizontal position using the surface grid. This method, described in [18], gives the surface value (z_{est}) given x and y.

$$z_{est}(x,y) = (1-t)(1-u)z_{i,j} + t(1-u)z_{i+1,j} + (1-t)uz_{i,j+1} + tuz_{i+1,j+1} \tag{3.1}$$

where $x_i < x < x_{i+1}$ and $y_j < y < y_{j+1}$, and

$$t = \frac{(x - x_i)}{(x_{i+1} - x_i)} \tag{3.2}$$

$$u = \frac{(y - y_j)}{(y_{j+1} - y_j)} \tag{3.3}$$

This method will be used in many of the algorithms developed as a tool to calculate the height on the surface grid.

3.5 Basic Formation of ILS Terms

Creation of the basic vectors and matrices for this research is described below. A normal epoch-by-epoch ILS structure will be introduced, and then this basic structure will be modified for the various algorithms that are implemented.

The measurements that will be used primarily in this research are single differenced carrier phase measurements. Assuming there are 5 pseudolites (labeled PRNS 1 through 5), one pseudolites is selected as the base transmitter for differencing. The measurements from the remaining transmitters will each be subtracted from the base transmitter's measurements. With PRN 1 designated as the base transmitter the measurement vector will appear as

$$\mathbf{z} = \left[\nabla\phi^{12}_{mob}\ \nabla\phi^{13}_{mob}\ \nabla\phi^{14}_{mob}\ \nabla\phi^{15}_{mob}\right]^T \tag{3.4}$$

where the single difference (∇) measurements are described by Equation (2.7). The tropospheric error is removed using the error model described in [11]. The psueudolite clock error is removed due to Locata synchronization, while the multipath and measurement noise terms are combined into the noise term. Under these assumptions, an individual measurement equation can be expressed as

$$= \lambda^{-1}(\nabla r^{12}_A) + \nabla N^{12}_A + \nu \tag{3.5}$$

where

$$\begin{aligned} \nu \quad &= \text{noise term} \\ \nabla N^{12}_A \quad &= \text{ambiguity term for } \nabla\phi^{12}_A \\ \nabla r^{12}_A \quad &= \text{single difference range} \end{aligned}$$

and ∇r_A^{12} can be represented as

$$\nabla r_A^{12} = \sqrt{(x_1 - x_A)^2 + (y_1 - y_A)^2 + (z_1 - z_A)^2} - \sqrt{(x_2 - x_A)^2 + (y_2 - y_A)^2 + (z_2 - z_A)^2} \tag{3.6}$$

$$\tag{3.7}$$

$[x_1, y_1, z_1]$,$[x_2, y_2, z_2]$, and $[x_A, y_A, z_A]$ are the positions of pseudolite 1, pseudolite 2, and receiver A, respectively.

The state vector, $\mathbf{x}$, contains the positions of the reciever and all of the ambiguity states for the entire batch process. The state vector corresponding to the above measurement vector is

$$\mathbf{x} = \begin{bmatrix} x_A & y_A & z_A & \nabla N_A^{12} & \nabla N_A^{13} & \nabla N_A^{14} & \nabla N_A^{15} \end{bmatrix}^T \tag{3.8}$$

The right hand side of Equation (3.5) contains the differenced range from the estimated receiver position to two transmitters. Equation (3.5) can be expressed in the form $\mathbf{z} = h(\mathbf{x}) + \nu$, where

$$h_A^{12}(\mathbf{x}) = \lambda^{-1}(\sqrt{(x_1 - x_A)^2 + (y_1 - y_A)^2 + (z_1 - z_A)^2} - \sqrt{(x_2 - x_A)^2 + (y_2 - y_A)^2 + (z_2 - z_A)^2}) + \nabla N_A^{12} \tag{3.9}$$

Formulation of the $\mathbf{H}$ matrix is done by finding the partial derivatives of $h_A^{12}(\mathbf{x})$ wrt the state vector.

This is shown for a single row of the $\mathbf{H}$ matrix as an example.

$$\left.\frac{\partial h_A^{12}(\mathbf{x})}{\partial x_A}\right|_{\hat{\mathbf{x}}} = -\frac{1}{\lambda}\left\{\frac{x_1-x_A}{[(x_1-x_A)^2+(y_1-y_A)^2+(z_1-z_A)^2]^{1/2}}\right\} + \frac{1}{\lambda}\left\{\frac{x_2-x_A}{[(x_2-x_A)^2+(y_2-y_A)^2+(z_2-z_A)^2]^{1/2}}\right\} = \frac{1}{\lambda}\{-e_x^1+e_x^2\} \tag{3.10}$$

$$\left.\frac{\partial h_A^{12}(\mathbf{x})}{\partial y_A}\right|_{\hat{\mathbf{x}}} = -\frac{1}{\lambda}\left\{\frac{y_1-y_A}{[(x_1-x_A)^2+(y_1-y_A)^2+(z_1-z_A)^2]^{1/2}}\right\} + \frac{1}{\lambda}\left\{\frac{y_2-y_A}{[(x_2-x_A)^2+(y_2-y_A)^2+(z_2-z_A)^2]^{1/2}}\right\} = \frac{1}{\lambda}\{-e_y^1+e_y^2\} \tag{3.11}$$

$$\left.\frac{\partial h_A^{12}(\mathbf{x})}{\partial z_A}\right|_{\hat{\mathbf{x}}} = -\frac{1}{\lambda}\left\{\frac{z_1-z_A}{[(x_1-x_A)^2+(y_1-y_A)^2+(z_1-z_A)^2]^{1/2}}\right\} + \frac{1}{\lambda}\left\{\frac{z_2-z_A}{[(x_2-x_A)^2+(y_2-y_A)^2+(z_2-z_A)^2]^{1/2}}\right\} = \frac{1}{\lambda}\{-e_z^1+e_z^2\} \tag{3.12}$$

$$\left.\frac{\partial h_A^{12}(\mathbf{x})}{\partial \nabla N_A^{12}}\right|_{\hat{\mathbf{x}}} = 1 \tag{3.13}$$

where

$$\mathbf{e}_A^j = [e_x^j \; e_y^j \; e_z^j] \tag{3.14}$$

is the unit line-of-sight vectors pointing from the mobile receiver to pseudolite j.

Forming these partial derivatives into the complete $\mathbf{H}$ matrix for a single epoch is

$$\mathbf{H} = \begin{bmatrix} \frac{1}{\lambda}(-\mathbf{e}^1+\mathbf{e}^2) & 1 & 0 & 0 & 0 \\ \frac{1}{\lambda}(-\mathbf{e}^1+\mathbf{e}^3) & 0 & 1 & 0 & 0 \\ \frac{1}{\lambda}(-\mathbf{e}^1+\mathbf{e}^4) & 0 & 0 & 1 & 0 \\ \frac{1}{\lambda}(-\mathbf{e}^1+\mathbf{e}^5) & 0 & 0 & 0 & 1 \end{bmatrix} \tag{3.15}$$

where $\mathbf{e}^j$ is the unit line-of-sight vector between the mobile receiver and pseudolite j.

The measurement covariance matrix, $\mathbf{R}$, is a square matrix with diagonal terms corresponding to the noise variance in each measurement and off-diagonal terms corresponding to the cross-covariances between measurements. Carrier-phase measurements are the only measurements being considered in this example. Carrier-phase cross-covariances are assumed to be half of the carrier-phase variance, because half of the measurements are in common due to differencing [8].

$$\mathbf{R} = \begin{bmatrix} \sigma_\phi^2 & \frac{\sigma_\phi^2}{2} & \frac{\sigma_\phi^2}{2} & \frac{\sigma_\phi^2}{2} \\ \frac{\sigma_\phi^2}{2} & \sigma_\phi^2 & \frac{\sigma_\phi^2}{2} & \frac{\sigma_\phi^2}{2} \\ \frac{\sigma_\phi^2}{2} & \frac{\sigma_\phi^2}{2} & \sigma_\phi^2 & \frac{\sigma_\phi^2}{2} \\ \frac{\sigma_\phi^2}{2} & \frac{\sigma_\phi^2}{2} & \frac{\sigma_\phi^2}{2} & \sigma_\phi^2 \end{bmatrix} \tag{3.16}$$

where $\sigma_\phi^2 = .004\ m^2$ [20].

From the example supplied it is important to note the number of states and the number of measurements. Given the 5 pseudolites, there are 4 single differenced measurements available. With 3 position states and one ambiguity state for each measurement, the number of states reaches 7. It is not possible to accurately estimate 7 states from only 4 measurements. The solution to this problem lies in the commonality of the ambiguities. Assuming there are no cycle slips, the same ambiguity state is associated with all the measurements from a single transmitter. A batch ILS process will allow measurements from multiple times to be used in estimating the position of the receiver at each time as well as the ambiguity state common to the measurements across different times.

3.5.1 Batch processing. For a batch ILS estimation problem the above single-epoch example will be expanded. Instead of using the measurements from a single time epoch, measurements from multiple epochs will be used. The states associated with each time epoch will also be used to create a single larger state vector. Consider using the same number of pseudolites as in the previous section, but now

instead of using only a single time, three times will be used. The measurement and state vectors will now appear as

$$\mathbf{z} = \left[\nabla\phi_{t1}^{12}\ \nabla\phi_{t1}^{13}\ \nabla\phi_{t1}^{14}\ \nabla\phi_{t1}^{15}\ \nabla\phi_{t2}^{12}\ \nabla\phi_{t2}^{13}\ \nabla\phi_{t2}^{14}\ \nabla\phi_{t2}^{15}\ \nabla\phi_{t3}^{12}\ \nabla\phi_{t3}^{13}\ \nabla\phi_{t3}^{14}\ \nabla\phi_{t3}^{15}\right]^T \tag{3.17}$$

$$\mathbf{x} = \left[x_{t1}\ y_{t1}\ z_{t1}\ x_{t2}\ y_{t2}\ z_{t2}\ x_{t3}\ y_{t3}\ z_{t3}\ \nabla N^{12}\ \nabla N^{13}\ \nabla N^{14}\ \nabla N^{15}\right]^T \tag{3.18}$$

where subscripts t_1, t_2, and t_3 indicate the time epochs for the particular measurement or state. It is assumed that there are no cycle slips, so the ambiguities remain valid for all three epochs. It is noted that instead of estimating 7 states with 4 measurements (as in the single epoch example), now 13 states are being estimated with 12 measurements. If more epochs were considered in the batch process, the number of states will be smaller than the number of measurements, and accurate estimation of the states can be accomplished.

The batch **H** matrix is a block diagonal combination of single-epoch **H** matrices (from Equation 3.15), with ambiguity terms (1's) consolidated in the last 4 columns, as shown below

$$\mathbf{H} = \begin{bmatrix} \frac{1}{\lambda}(-\mathbf{e}^1_{t1} - \mathbf{e}^2_{t1}) & [0,0,0] & [0,0,0] & 1 & 0 & 0 & 0 \\ \frac{1}{\lambda}(-\mathbf{e}^1_{t1} - \mathbf{e}^3_{t1}) & [0,0,0] & [0,0,0] & 0 & 1 & 0 & 0 \\ \frac{1}{\lambda}(-\mathbf{e}^1_{t1} - \mathbf{e}^4_{t1}) & [0,0,0] & [0,0,0] & 0 & 0 & 1 & 0 \\ \frac{1}{\lambda}(-\mathbf{e}^1_{t1} - \mathbf{e}^5_{t1}) & [0,0,0] & [0,0,0] & 0 & 0 & 0 & 1 \\ [0,0,0] & \frac{1}{\lambda}(-\mathbf{e}^1_{t2} + \mathbf{e}^2_{t2}) & [0,0,0] & 1 & 0 & 0 & 0 \\ [0,0,0] & \frac{1}{\lambda}(-\mathbf{e}^1_{t2} + \mathbf{e}^3_{t2}) & [0,0,0] & 0 & 1 & 0 & 0 \\ [0,0,0] & \frac{1}{\lambda}(-\mathbf{e}^1_{t2} + \mathbf{e}^4_{t2}) & [0,0,0] & 0 & 0 & 1 & 0 \\ [0,0,0] & \frac{1}{\lambda}(-\mathbf{e}^1_{t2} + \mathbf{e}^5_{t2}) & [0,0,0] & 0 & 0 & 0 & 1 \\ [0,0,0] & [0,0,0] & \frac{1}{\lambda}(-\mathbf{e}^1_{t3} + \mathbf{e}^2_{t3}) & 1 & 0 & 0 & 0 \\ [0,0,0] & [0,0,0] & \frac{1}{\lambda}(-\mathbf{e}^1_{t3} + \mathbf{e}^3_{t3}) & 0 & 1 & 0 & 0 \\ [0,0,0] & [0,0,0] & \frac{1}{\lambda}(-\mathbf{e}^1_{t3} + \mathbf{e}^4_{t3}) & 0 & 0 & 1 & 0 \\ [0,0,0] & [0,0,0] & \frac{1}{\lambda}(-\mathbf{e}^1_{t3} + \mathbf{e}^5_{t3}) & 0 & 0 & 0 & 1 \end{bmatrix} \tag{3.19}$$

The batch $\mathbf{R}$ matrix is also a block diagonal combination of single-epoch $\mathbf{R}$ matrices as shown below

$$\mathbf{R} = \begin{bmatrix} \sigma^2_\phi & \frac{\sigma^2_\phi}{2} & \frac{\sigma^2_\phi}{2} & \frac{\sigma^2_\phi}{2} & 0 & 0 & 0 & 0 & 0 & 0 & 0 & 0 \\ \frac{\sigma^2_\phi}{2} & \sigma^2_\phi & \frac{\sigma^2_\phi}{2} & \frac{\sigma^2_\phi}{2} & 0 & 0 & 0 & 0 & 0 & 0 & 0 & 0 \\ \frac{\sigma^2_\phi}{2} & \frac{\sigma^2_\phi}{2} & \sigma^2_\phi & \frac{\sigma^2_\phi}{2} & 0 & 0 & 0 & 0 & 0 & 0 & 0 & 0 \\ \frac{\sigma^2_\phi}{2} & \frac{\sigma^2_\phi}{2} & \frac{\sigma^2_\phi}{2} & \sigma^2_\phi & 0 & 0 & 0 & 0 & 0 & 0 & 0 & 0 \\ 0 & 0 & 0 & 0 & \sigma^2_\phi & \frac{\sigma^2_\phi}{2} & \frac{\sigma^2_\phi}{2} & \frac{\sigma^2_\phi}{2} & 0 & 0 & 0 & 0 \\ 0 & 0 & 0 & 0 & \frac{\sigma^2_\phi}{2} & \sigma^2_\phi & \frac{\sigma^2_\phi}{2} & \frac{\sigma^2_\phi}{2} & 0 & 0 & 0 & 0 \\ 0 & 0 & 0 & 0 & \frac{\sigma^2_\phi}{2} & \frac{\sigma^2_\phi}{2} & \sigma^2_\phi & \frac{\sigma^2_\phi}{2} & 0 & 0 & 0 & 0 \\ 0 & 0 & 0 & 0 & \frac{\sigma^2_\phi}{2} & \frac{\sigma^2_\phi}{2} & \frac{\sigma^2_\phi}{2} & \sigma^2_\phi & 0 & 0 & 0 & 0 \\ 0 & 0 & 0 & 0 & 0 & 0 & 0 & 0 & \sigma^2_\phi & \frac{\sigma^2_\phi}{2} & \frac{\sigma^2_\phi}{2} & \frac{\sigma^2_\phi}{2} \\ 0 & 0 & 0 & 0 & 0 & 0 & 0 & 0 & \frac{\sigma^2_\phi}{2} & \sigma^2_\phi & \frac{\sigma^2_\phi}{2} & \frac{\sigma^2_\phi}{2} \\ 0 & 0 & 0 & 0 & 0 & 0 & 0 & 0 & \frac{\sigma^2_\phi}{2} & \frac{\sigma^2_\phi}{2} & \sigma^2_\phi & \frac{\sigma^2_\phi}{2} \\ 0 & 0 & 0 & 0 & 0 & 0 & 0 & 0 & \frac{\sigma^2_\phi}{2} & \frac{\sigma^2_\phi}{2} & \frac{\sigma^2_\phi}{2} & \sigma^2_\phi \end{bmatrix} \tag{3.20}$$

3.6 Algorithms

Once the data has been analyzed for cycle slips using the SNR measurements, the ambiguity states can be associated with the measurements. The initial trajectory is calculated using the pseudorange measurements. After this is done, the epoch selection process is done to determine which times will be used to form the batch process. Next, the batch ILS process is used to estimate the ambiguity states. During the ILS estimation, the tropospheric delay is modelled and subtracted from the measurements. Finally, once the ambiguities are known, the final solution can be found epoch by epoch using the ILS algorithm.

Figure 3.6 illustrates the overall process described above in a block diagram. This process is followed for each height aiding algorithm. The process is the same for using either true data or simulated data. With true data, the surface grid is computed from the GPS truth positions, while in simulated data the grid is set. The simulated data is also generated in the ENU frame so that any frame rotations required for real data are not needed.

In common practice, the solution is constrained to the horizontal plane. A nominal height is assumed and the problem is now reduced to finding the horizontal positions. In most cases for which height constraints are used, the height is known. In this research the receiver is travelling on a known surface. The height is therefore known if the horizontal positions are known. The following sections will provide the presentation of the five algorithms developed to use the known topography to aid the ILS estimation in this research.

3.6.1 Method 1: Horizontal Solution Constrained to the Surface. The first method will assume an initial position, including an initial height. This solution will be used as the linearization point for the $\mathbf{H}$ matrix. The problem will then be constrained to the horizontal plane by removing the height from the state vector and removing the corresponding column from the $\mathbf{H}$ matrix. It is important to note that the full 3-d position will be used to calculate the measurement residuals $\Delta\mathbf{z}$.

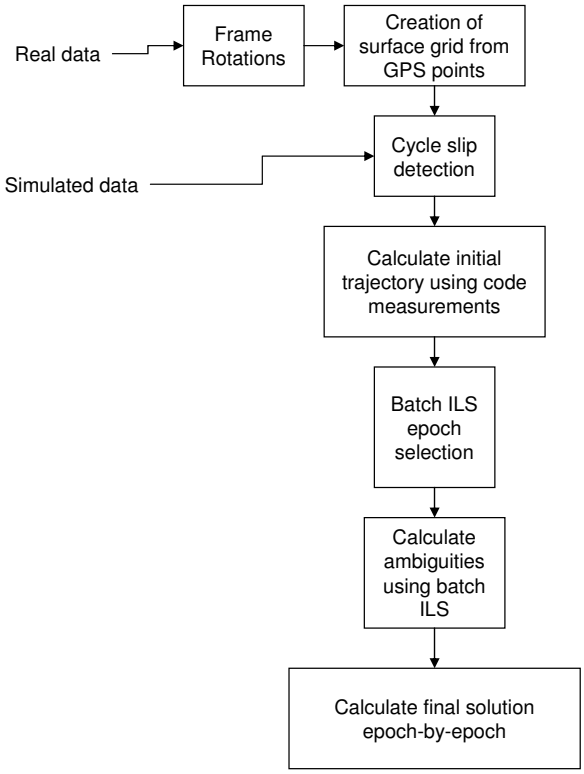

Figure 3.6: Block diagram of overall algorithm process.

In this manner the initial height will not be estimated in the ILS process. The updates to the states will be calculated and used to create the new position for the beginning of the next iteration. Once the new states are determined and before the next iteration starts, the horizontal components of the position will be used to find their corresponding height on the grid. This height will be determined by using the known topography grid.

The horizontal components are used to find the four surrounding grid points. Bilinear interpolation is then used to find the height that matches the horizontal components. Once this new height is found, the process starts again. In this manner, the solution will always lie on the surface.

This method estimates only the horizontal components of the receiver position. This is important in considering the number of states that will be estimated and thus the size of the matrix inversion required in the ILS process. Each epoch that

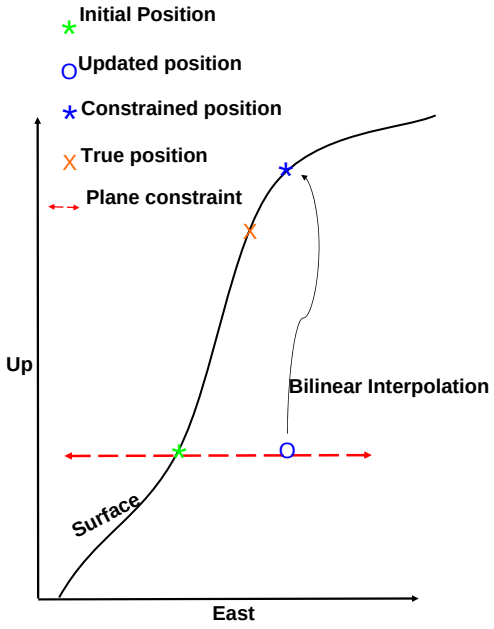

Figure 3.7: Illustration of Method 1.

is included in the batch process will contribute 2 position states. While the number of position states estimated will change with each method, the number of ambiguity states estimated will remain the same between the different methods.

An illustration of how Method 1 might converge to a solution is given in Figure 3.7. The iteration begins with an initial position (green star). The height is held constant at the initial height, while the horizontal position is estimated. Once the estimation process has updated the initial position (only the horizontal points), the solution is constrained to lie on the surface using bilinear interpolation. Once the new height is found using the surface grid the process begins again. This is done until a solution is converged upon.

3.6.2 Method 2: 3-D solution with pseudo-measurement. The second algorithm tested more directly follows the common height constraint methods [17, 23, 27]. A pseudo-measurement of the height is created based upon the bilinear interpolation

of the current location on the grid (Equation (3.1)). The measurement is incorporated alongside the single-differenced phase measurements. This allows the solution to be found in 3-dimensions. A variance is associated with the height measurement and is augmented to the existing measurement noise covariance. This variance is chosen to be $(.001m)^2$. This assumes the grid is accurate to 1 mm. A 1 mm error is acceptable, since the truth height will also be fitted to the surface grid using the same interpolation method. Each position calculated during the iteration process is used to create a pseudo-measurement of the height based on the pre-formed grid. This pseudo-measurement will be used in the next iteration. Instead of limiting the ILS estimate to only the horizontal positions, it is now able to estimate all 3 position states.

Estimating 3 position states instead of 2 will increase the size of the required matrix by roughly 50 percent. For instance, a batch process of 100 epochs, with a total of 10 ambiguity states, will invoke a 210 by 210 matrix inversion using method 1, and a 310 by 310 matrix inversion using Method 2.

Given the same conditions described in previous sections, but with a pseudo-measurement now available, the **H** matrix will contain an additional row corresponding to the new measurement. Since the height measurement is a direct measure of the height component, its partial derivatives wrt any other states are zero. Thus, if the state vector contains the three positions states, and four ambiguity states the row appended to the **H** matrix will be [0 0 1 0 0 0 0]. A new diagonal entry will be added to the measurement noise matrix, **R**, as well:

$$\mathbf{R}_{method_2} = \begin{bmatrix} & & & \vdots \\ & \mathbf{R} & & 0 \\ & & & \vdots \\ \cdots & 0 & \cdots & \sigma^2_{HC} \end{bmatrix} \tag{3.21}$$

where a value of $\sigma^2_{HC} = (0.001m)^2$ was chosen since the surface grid was created using DGPS.

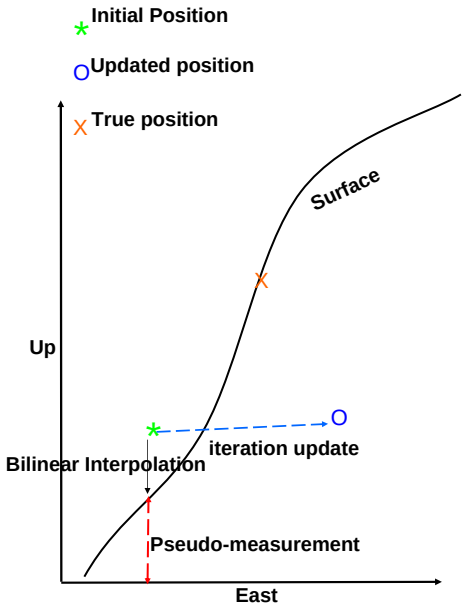

Figure 3.8: Illustration of Method 2.

Again, an illustration will be used to show how Method 2 behaves (Figure **??**). This algorithm does not require that the solution lies on the surface. Before estimation occurs, the horizontal positions of the initial point are used to measure the height of the surface at that point using bilinear interpolation. This pseudo-measurement is incorporated into the solution process. The height constraint really attempts to force the solution to stay near the height of the surface known from the last iteration. The new solution is estimated in three dimensions.

3.6.3 Method 3: Single Value Decomposition Epoch-by-Epoch Transformation. Problems can occur in ILS when the rank of $\mathbf{H}$ is less than the number of states. This will cause the matrix $\mathbf{H}^T\mathbf{H}$ to be singular and uninvertible.

Another problem occurs when a state parameter is nearly unobservable. While there is no rank deficiency causing the problem of uninvertiblity, the estimate of the unobservable state will be poor. To eliminate this problem, the state space of the

system can be transformed to eliminate the problem states. The transformation will change both the state vector and the $\mathbf{H}$ matrix as shown.

$$\mathbf{x}^{'}_{n' \times 1} = \mathbf{T}_{n' \times n} \mathbf{x}_{n \times 1} \tag{3.22}$$

$$\mathbf{H}^{'}_{m \times n'} = \mathbf{H}_{m \times n} \left(\mathbf{T}^{T} \right)_{n \times n'} \tag{3.23}$$

where $n^{'} < n$ and the prime notation indicate the new state vector and $\mathbf{H}^{'}$ matrix. The above and following derivation closely follow the development given in [21]. It is also very similar to the concept of primary component analysis [12].

3.6.3.1 Transformation matrix. Determining the transformation matrix to use is accomplished by exploiting the method of SVD. First, the singular value decomposition of $\mathbf{H}$ is generated

$$\mathbf{H} = \mathbf{U} \mathbf{\Sigma} \mathbf{V}^{T} \tag{3.24}$$

where

$$\mathbf{U} = \begin{bmatrix} \uparrow & \uparrow & & \uparrow \\ \mathbf{u}_1 & \mathbf{u}_2 & \cdots & \mathbf{u}_m \\ \downarrow & \downarrow & & \downarrow \end{bmatrix} \tag{3.25}$$

in which $\mathbf{u}_i$'s are left singular vectors of $\mathbf{H}$ (the right eigenvectors of $\mathbf{H}\mathbf{H}^{T}$),

$$\mathbf{V} = \begin{bmatrix} \uparrow & \uparrow & & \uparrow \\ \mathbf{v}_1 & \mathbf{v}_2 & \cdots & \mathbf{v}_n \\ \downarrow & \downarrow & & \downarrow \end{bmatrix} \tag{3.26}$$

where $\mathbf{v}_i$'s are right singular vectors of $\mathbf{H}$ (the right eigenvectors of $\mathbf{H}^T\mathbf{H}$), and

$$\mathbf{\Sigma} = \begin{bmatrix} \sigma_1 & & & 0 \\ & \sigma_2 & & \\ & & \ddots & \\ 0 & & & \sigma_n \end{bmatrix} \tag{3.27}$$

where $\sigma_1 \geq \sigma_2 \geq \ldots \geq \sigma_n \geq 0$ are the singular values of $\mathbf{H}$ (the square roots of the eigenvalues of $\mathbf{H}^T\mathbf{H}$).

Consider the $\mathbf{H}$ as a mapping function that maps the state vector into the measurement vector. The SVD of $\mathbf{H}$ gives an orthonormal basis for $\mathbf{H}^T\mathbf{H}$ (the right singular vectors, $\mathbf{v}_i$'s) and a measure of the observability of each basis vector (the singular values, σ_i's). Small singular values are indicators of unobservability. Creating the transformation matrix is as simple as eliminating the right singular vectors that correspond to the deficient singular values. As an example, suppose there are n singular values, selecting k of the largest singular values, where $k < n$ would yield a transformation matrix of

$$\mathbf{T} = \begin{bmatrix} \leftarrow & \mathbf{v}_1^T & \rightarrow \\ \leftarrow & \mathbf{v}_2^T & \rightarrow \\ & \vdots & \\ \leftarrow & \mathbf{v}_k^T & \rightarrow \end{bmatrix} \tag{3.28}$$

Now, this $\mathbf{T}$ matrix can be used to transform the $\mathbf{H}$ matrix and the state vector as shown in Equations (3.22) and (3.23). Using the new $\mathbf{H}'$ matrix and state vector, perform the same ILS method. Once the transformed states have been estimated the same transformation matrix can be used to find the original state vector.

$$\mathbf{x} = \mathbf{T}^T\mathbf{x}' \tag{3.29}$$

When transforming back to the original state space, the estimate of the states that were eliminated due to near unobservability will still be poor. This creates the need for these states to be estimated using the known surface grid, just as in Method 1.

Method 3 will use the above SVD approach to change the states of the batch process through an epoch-by-epoch formulation. As previously mentioned, the batch process can be conceptualized as a combination of single epochs into one ILS process. The SVD approach can be used at each epoch to transform the block diagonal components of the batch **H** matrix. These block diagonal components are initially related to the three ENU position states of a single epoch. The SVD approach will transform the states into the principal directions and eliminate the least observable state. For a ground-based system this is usually the vertical state. It is assumed in this method that there is a deficiency in the vertical direction.

At each epoch, the SVD approach will be used to transform the states for that epoch alone. This will be done for each epoch included in the batch process. After this is done, the batch **H** matrix is created using the **H** matrix from each epoch.

In this method the lowest singular value will be selected and its corresponding state will be eliminated. This will always constrain the solution to the optimal plane determined by the SVD approach. Accordingly, the size of the matrix inversion required in the batch ILS process is the same size as in Method 2.

Figure **??** shows how Method 3 constrains the solution to lie on a plane (similar to Method 1). The difference is that the plane in this method is formed to eliminate the least observable direction. The SVD approach will transform the state space into a 2-D plane and continue to iterate similar to Method 1. The difference only lies in the alignment of the planes.

3.6.4 Method 4: Single Value Decomposition Batch Transformation. Instead of using the SVD approach on each individual epoch of the batch process, it is possible to transform the entire state vector and **H** matrix. The same method of SVD is applied as in the epoch by epoch approach above. It is important to note that in this case

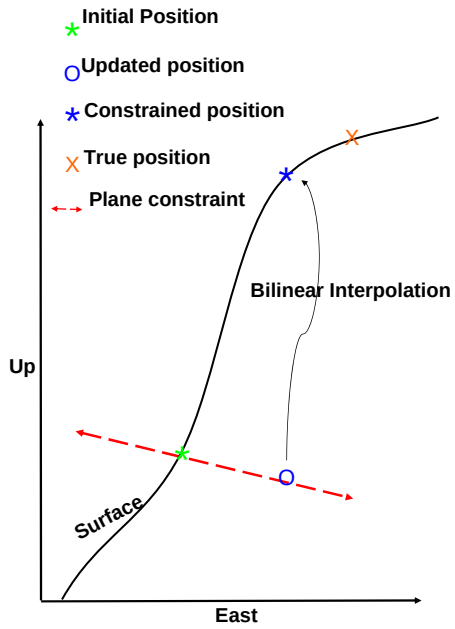

Figure 3.9: Illustration of Method 3.

a threshold is set to determine which singular values and thus which singular vectors will be used to form the transformation matrix. The threshold is selected so that the solution does not have invertibility issues. This means the third dimension will not be automatically removed unless the singular value associated with it is below the threshold.

The surface information will be applied at the end of each iteration using the same bilinear interpolation method as in the previous methods. Once the states have been transformed back to the original ENU representation the height can be constrained to lie on the surface using the two horizontal components.

This method differs from the previous SVD method in its implementation on the entire batch process at once and its use of a threshold. The threshold will allow the SVD process to only eliminate states that have singular values below a threshold and more likely to have true observability deficiencies. Considering the entire batch

process at once can allow the observability of states to depend upon information from other epochs other than their own associated time. Since there is no constraint on the number of states that are eliminated, there is no set size to the matrix inversion in the ILS calculation, other than the maximum number being 3 states per epoch and the original number of ambiguity states.

Since this method does not force the constraining of the solution to a plane, there cannot be an easy visualization of its solution process. This method also transforms all the position states from all the epochs at once. This could allow the constraint to be much different than before. In essence the transformation will always align the new state space with the directions of most observability.

3.6.5 Method 5: Tangent Plane Transformation. This method takes advantage of the topographical surface in a different manner than the previous methods. Instead of constraining the height of the solution or finding the optimal plane dependent of the location of the pseudolites and receiver, this approach constrains the solution to a plane tangent to the known surface.

Finding the plane tangent to the surface grid is accomplished by finding a basis for the plane using 3 points. The current solution position will be used as the origin of the basis. A second point is found by moving a small distance in the east direction and finding the associated height using bilinear interpolation. Another point is found by making a small change in the north direction and finding its corresponding height. Using the center point and each of the two calculated points, two orthogonal vectors are created. Next the unit vectors in these directions are found and used as the basis vectors for the new solution plane. Since these vectors are orthogonal, they can be defined as the vectors [1,0,0] and [0,1,0] in our new frame. A transformation matrix into this new plane is then created by representing these basis vectors in the original coordinate frame. This method of coordinate frame transformation is described in [13].

The state vector and the **H** matrix are transformed similarly to Method 3 for each epoch. The solution is constrained to lie on the tangent plane. Once the solution

is found, it must be transformed back to the original ENU frame. As in the SVD methods, the transformation cannot create a good estimate of the height without additional information. Therefore the height is still constrained to lie on the surface grid before the next iteration begins.

This method constrains the solution to two dimensions. This will allow the size of the required matrix inversion in the ILS process to be roughly 33 percent smaller than a normal 3 dimensional solution method.

The illustration of this method is shown in Figure **??**. This method constrains the solution to a plane as in Methods 1 and 3, but the plane is now found to be tangent to the known surface. This aligns the state space with the direction of slope of the terrain. The iteration process is similar to Methods 1 and 3. An initial position is considered. This position is used to find the tangent plane and transformation matrix. The transformation is used to constrain the state space to the plane. The solution is found and then constrained again to the surface using bilinear interpolation. Once this has occurred, a new iteration can continue.

3.7 Test Setups

The following section will detail the setup for the real world test as well as the different simulations.

3.7.1 Real Road Test. A real test using five LocataLites was conducted at the Locata test facility. The locations for the LocataLites are given in ECEF coordinates in Table 3.1. These coordinates were surveyed using Leica System 500 and 1200 GPS receivers and processed using Leica GEO Office [1]. A 2-D map looking down at the horizontal positions of the LocataLites and the road is shown in Figure 3.11.

The LocataLites surrounded the road on which the test was conducted. This setup had been created by the Locata engineers for the purpose of conducting tests on the road. A test vehicle was configured with a Locata receiver and two GPS

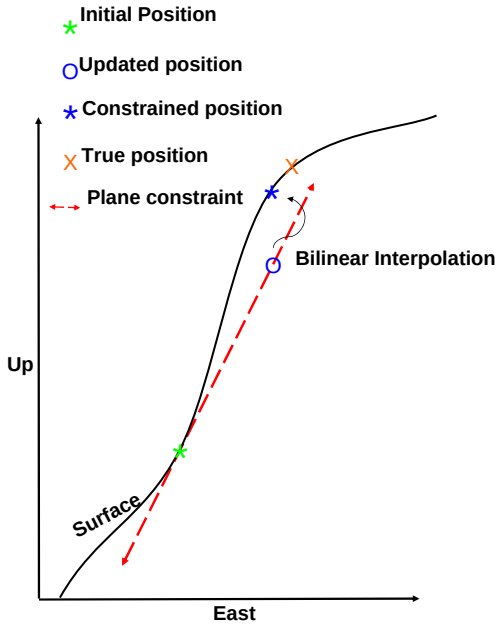

Figure 3.10: Illustration of Method 5.

antennas. The GPS antennas were mounted on either side of the Locata antenna. This would allow the truth position of the Locata receiver to be the mean of the two GPS positions. The GPS positions would be calculated using DGPS corrections from a fixed reference receiver.

The GPS receivers would not only provide a truth trajectory for comparison of the locata solutions, but would also be used to map the road for creation of the surface grid. This required multiple passes up and down the road so that a sufficient number

Table 3.1: ECEF locations for the LocataLites used during the real road test.

Name	PRN #	X (m)	Y (m)	Z (m)
South	1	-4431516.461	2635737.865	-3743255.799
West	2	-4431939.325	2636221.837	-3742211.816
North	3	-4432228.435	2636339.206	-3741769.434
Beach	4	-4432842.397	2635894.700	-3741362.460
East	5	-4432209.808	2635733.788	-3742244.268

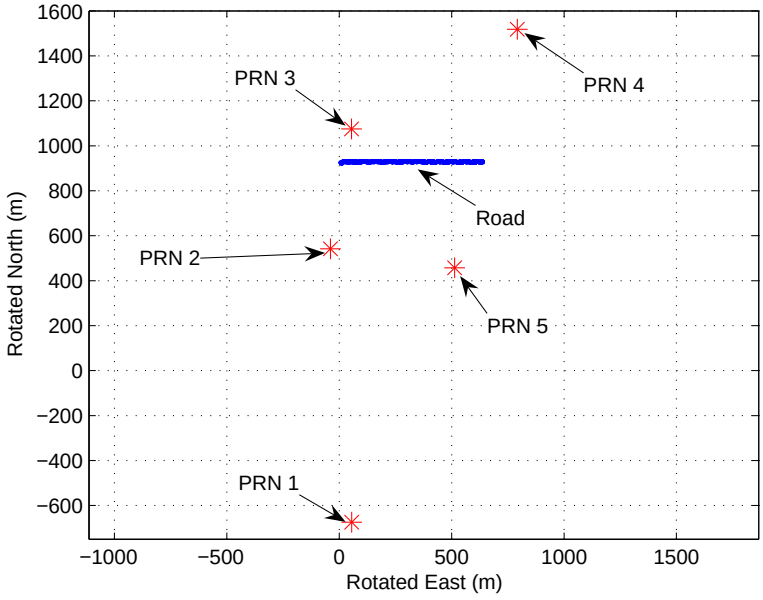

Figure 3.11: Horizontal view of the road test setup in the rotated ENU frame.

of points were collected for an accurate representation of the topography. Since data has been completely post processed, it was possible to collect GPS data for the grid and also data for the LocataLite system simultaneously. The primary test in this research is a meandering path that traverses up and down the length of the road.

3.7.2 Single Hill Simulations. A simple simulation is created by placing a hill at the origin of an ENU frame. The height and area of the hill can be changed to alter the slope of the hill. The position of the transmitters is also altered so as to create either good or poor geometries. A truth trajectory is chosen, which allows artificial measurements to be created. Either perfect measurements are used or white-Gaussian noise is added to the measurements. The truth trajectory need not be a realistic target trajectory, since the batch ILS approach does not assume any target dynamics.

This simulation is used to test how the different methods iterate to the final solutions. Methods will be compared on their final solution errors as well as the number of iterations involved in finding the solution. Different simulations can be

conducted using the same surface grid of a single hill. Instead of the truth positions all lying at the peak of the hill, the positions can be randomly scattered over the surface of the hill. Now starting from the same initial position at the top of the hill for each case, the simulation can test how the location of a truth point effects each algorithm. Individual simulations will be discussed with their corresponding results in the next chapter.

3.8 Summary

The details of the algorithms and calculation process have been discussed. The initial setup involved and differences in the proposed solutions has been introduced. In the next chapter the results from a real world test are discussed. Comparison of the different algorithms will also be presented.

IV. Analysis

4.1 Overview

In this section, results and analysis of the solutions will be presented. The first results shown are those from the real world testing that has been done. The issues that are associated with real measurements will be pointed out and discussed. After this, the analysis will shift to simulation data. Here, different methods can be compared by limiting the error parameters and choosing the initial and final positions.

4.2 Real Road Test

The road test was conducted as a proof-of-concept of a pseudolite-based system. The focus of this test is to show that centimeter level accuracy is attainable and to characterize issues in working with real data.

4.2.1 Solution Results. The road test conducted consisted of driving up and down the length of the road while swerving from side to side. Figure 4.1 shows the total three dimensional error in the solution using method 1. Figure 4.2 displays the 3 error components using method 1. There is a period of static testing (the vehicle was stationary such that the position data was highly accurate) done at the beginning of the run for roughly half of a minute. The graph shows the error under nine centimeters for the entire run. For most of the test the error is under 5 centimeters. Near five minutes into the test, the error jumps higher. Relating this graph to the Dilution of Precision plot in Figure 4.3, illustrates why there is a jump in the position errors. The geometry is least favorable near the end of the run. Despite the peak in the error, the mean error is 2.3 centimeters.

The road in this test is nearly flat. While this means there are no real problems in the solution process with any of the methods, it also means all of the methods behave nearly the same. There is little difference in the results for any of the methods.

Methods 1, 2, 3, and 5 all give nearly the exact same solutions (probably due to the flat road). Method 4 (SVD on the batch process), gives the only different solutions,

as shown in Figures 4.4 and 4.5. There is now a larger error in the middle of the run and the large error spike in the other methods around 5 minutes is lower in the results for Method 4. The mean error is still slightly above 2 centimeters. The difference in the solutions could be due to the number of dimensions used in method 4 for estimating its positions. Remember this method uses the SVD approach on the entire batch process and only eliminates states that correspond to singular values below a set threshold. This differes from the other methods which constrain the solution to a lower dimensionality. This inherently throws away some of the information in the measurements. In the case seen here, there may be times that the geometry still has decent observability and constraining the solution to two dimensions is not needed. This idea is captured in Method 4.

By breaking the 3-D error for Method 1 into components (see Figure 4.2), an interesting characteristic is seen in the east error. Looking at this east error, it can be seen to slowly rise and then fall. The error seems to grow as the receiver travels down the road and decreases on the way back. Although the tropospheric error has been decreased by the model applied, it appears that some residual tropospheric error is still present. As suggested in [8,9], the residual tropospheric error will be modelled as a scale factor on the original error. This is done for the real test and the results for method 1 are shown in Figures 4.6 and 4.7. The scale factor was estimated through iteration by hand. The goal being to reduce the error in the east direction toward zero. While the peak error is reduced slightly, the mean error increases to 2.7 centimeters. This indicates that the error model is incorrect. Research into modelling the residual tropospheric error and estimating potential Locatalite position errors is found in [24].

4.2.2 Finding Cycle Slips. Detecting cycle slips is crucial for correct determination of ambiguity states. If incorrect ambiguity states are related to the measurements, the precision of carrier-phase measurements is greatly decreased. As stated previously, cycle slips in GPS are often very dramatic and usually easily found. In the case of LocataLites, the errors can occur in such a way as to create a cycle drift

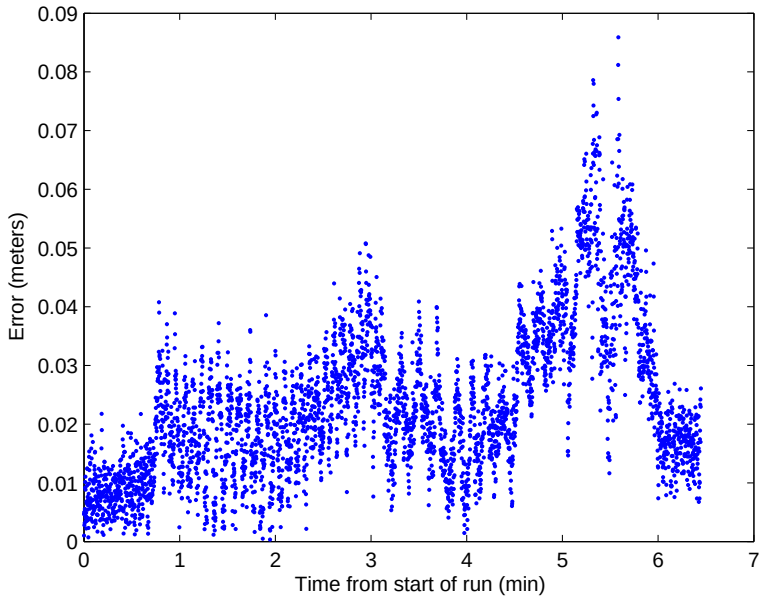

Figure 4.1: 3-D error for the road test using method 1.

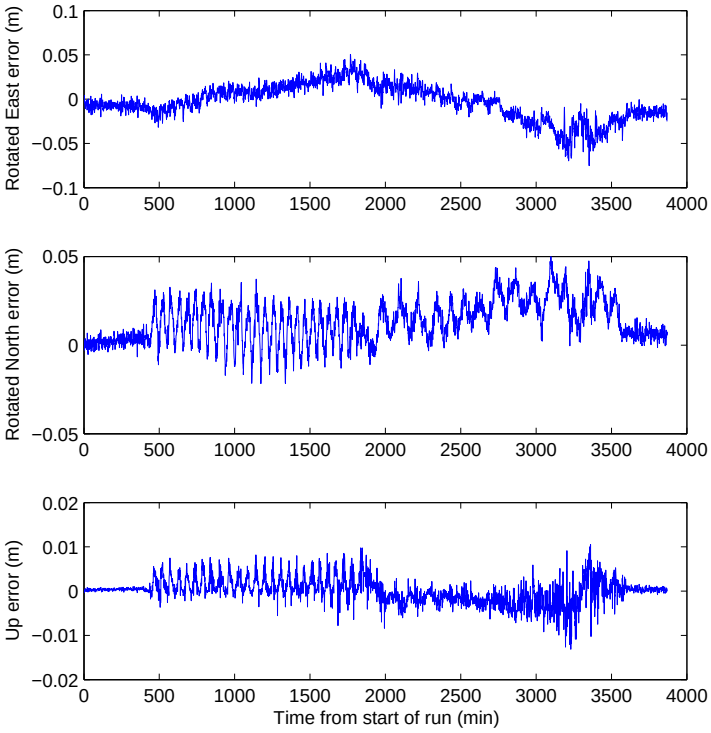

Figure 4.2: Error components for the road test using method 1.

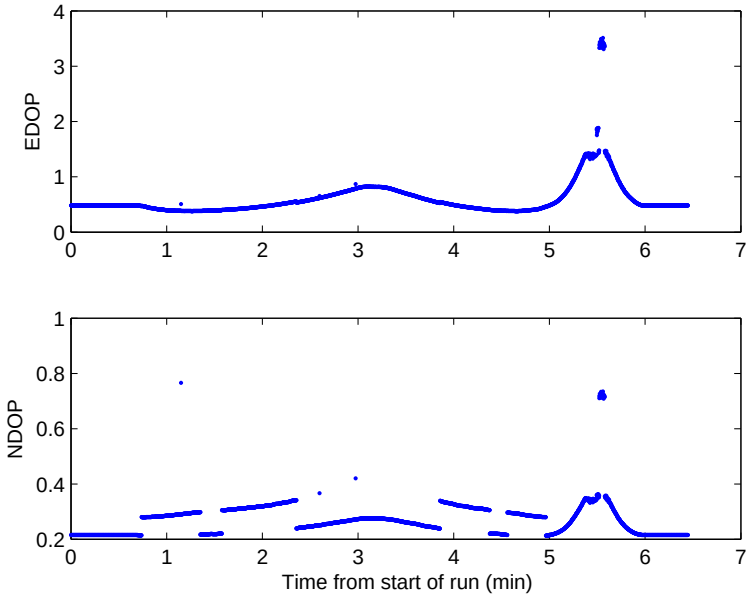

Figure 4.3: Dilution of Precision plot for the road test.

as opposed to an insatantaneous integer cycle slip. Monitoring SNR is the current method of determining cycle slips. A low SNR value indicates a potential cycle slip. When the SNR drops below a certain threshold it is assumed that a cycle slip has occured and a new ambiguity state is created. This method is appropriate assuming that the SNR is a good measure of when cycle slips occur.

Table 4.1 gives the estimates of the ambiguities for the road test. The PRN numbers are associated with the transmitter that is differenced with the base transmitter. The base transmitter in this case is PRN 4 and has no cycle slips (hence, its selection as the base). The start and stop epochs indicate the beginning and end of the ambiguities valid region of time. Note that the ambiguity estimates only changes by hundredths of a cycle for ambiguities 7 through 9. There is most likely no cycle slip causing the invalidation of the 7th ambiguity state and the creation of the 8th and 9th ambiguity state. An SNR measurement below the threshold has indicated there could be a cycle slip at some point in time causing these incorrect changes of ambiguity states. This anomaly is seen with PRNs 2 and 5 as well.

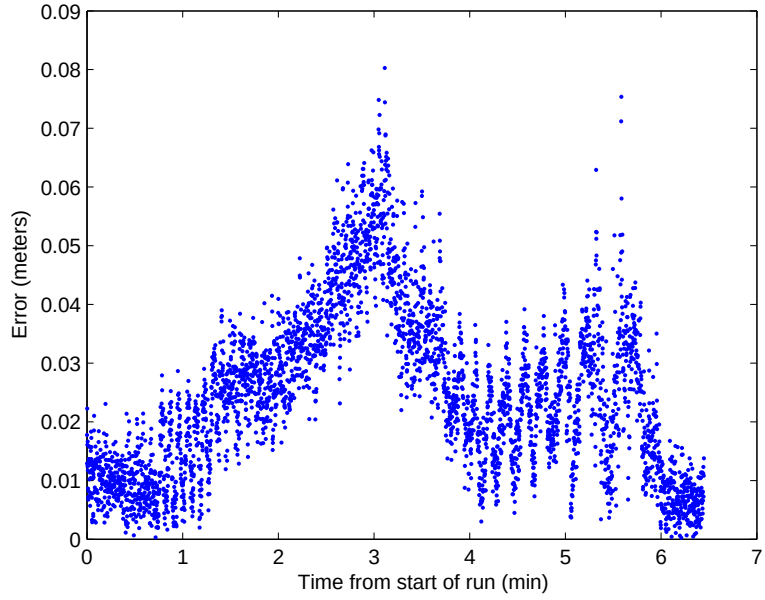

Figure 4.4: 3-D error for the road test using method 4.

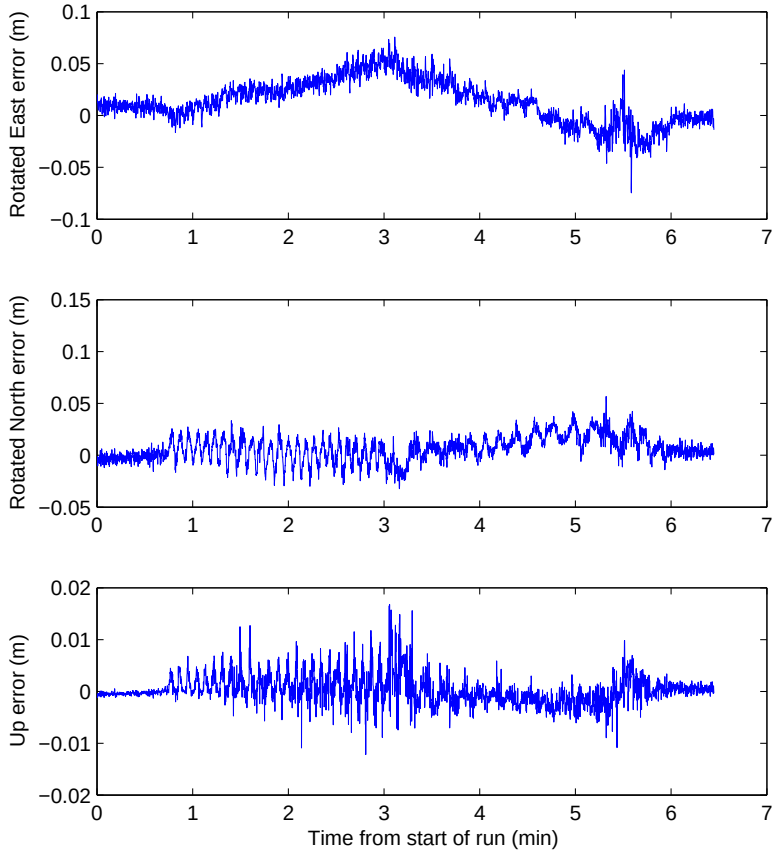

Figure 4.5: Error components for the road test using method 4.

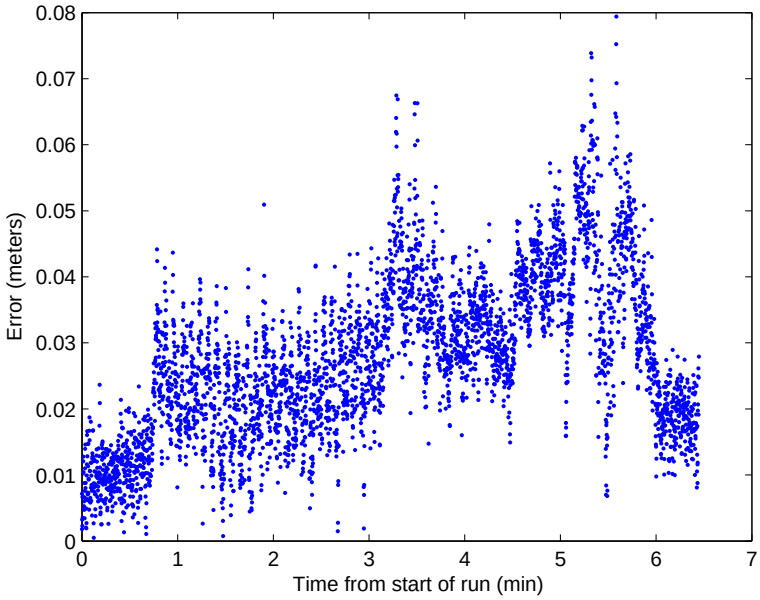

Figure 4.6: 3-D error for the road test using method 1 with the residual tropospheric error modelled as a scale factor.

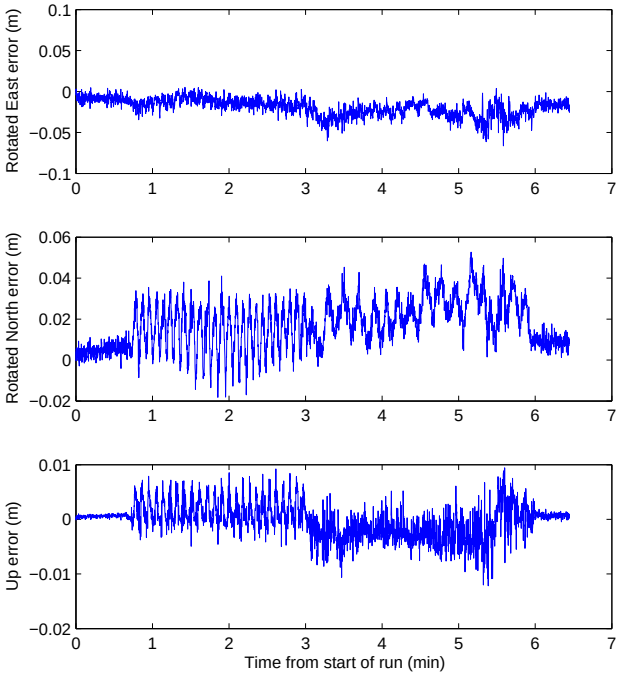

Figure 4.7: Component errors for the road test using method 1 with the residual tropospheric error modelled as a scale factor.

Table 4.1: Carrier-phase Ambiguity estimates for the road test.

Ambiguity State #	PRN #	Start Epoch	End Epoch	Ambiguity Estimate (cycles)
1	1	1	443	127265.794
2	2	1	3296	150088.190
3	3	1	3313	160819.296
4	5	1	690	164495.548
5	5	692	3869	164495.547
6	1	806	947	127307.689
7	1	1415	1559	127306.864
8	1	1561	1785	127306.881
9	1	1787	2314	127306.863
10	1	2627	2737	127308.228
11	1	2979	3869	127307.947
12	2	3309	3869	150088.292
13	3	3348	3869	160817.820

A further indication of the inadequacy of SNR measurements in indicating a cycle slip detection is shown in the solutions. Originally the position error using method 1 appeared as in Figures 4.8 and 4.9 instead of the position errors in Figures 4.1 and 4.2. There is a large spike early in the test run. A marker has been placed at the peak to show the epoch that it occurred. From analyzing the data it is apparent that an ambiguity state has just been created at this time. Referring to Table 4.1, ambiguity 6 can be seen as becoming valid at epoch 806. This means the measurements from PRN 1 that were not previously available due to an assumed cycle slip, are now being used. Including more measurements should improve the solution, and not cause a spike in the errors. Searching for the answer led to investigating the true measurement residuals.

The true measurement residuals are found by using the truth trajectory obtained from differential GPS. Given the truth trajectory the true measurements can be calculated. Differencing these true measurements with the actual measurements removes the effects of geometry changes from the actual measurements. The changes in the residuals therefore indicate the presence of other errors. Ambiguity changes

will be easily seen as well as tropospheric delays. Figure 4.10 shows the true measurement residuals. Matching the time of the error spike in the position error plot with the same time on the measurement residual plot shows the cause of the large error as being an ambiguity error.

The large error occurs while the measurement is still in a cycle drift, which can be seen as the large change in the measurement residuals over time. This large drift corresponds to transmitter 1. At this time an ambiguity state is being incorporated, based on good SNR measurements. The problem is that the cycle drift is still occurring and the ambiguity that is valid for later time periods is not valid at this time. This causes the large error that is seen. Looking at the component break down of the errors (Figure 4.9), the majority of the error spike is in the north direction. Since the ambiguity for transmitter 1 is incorrect, measurements from this pseudolite are going to cause an error in the solution. Refering to the locations of the transmitters (Figure 3.11), note that PRN 1 is the transmitter that has the best observability into the north direction. The fact that the error from the incorrect ambiguity effects the north primarily helps corroborate the theory that the cycle slip detection method is not identifying the correct slips.

The SNR measurements are good while a cycle slip is occurring. This is a very strong indication the SNR measurements are not adequate for tracking cycle slips for the system used in this test.

4.2.3 Grid Errors. In this research the surface topography was created using surveyed GPS points. The positions were gathered while driving the test vehicle to collect Locota receiver data. Efforts were made to combine enough GPS tracks to create an accurate representation of the road. Looking at some of the data suggests there are errors introduced when using a surface topography created from sparse GPS points. Figures 4.11 and 4.12 show the GPS trajectories plotted along with the road trajectory. The color of the road trajectory has been altered to show positions with medium and large error. Large errors are those that are above 66 percent of

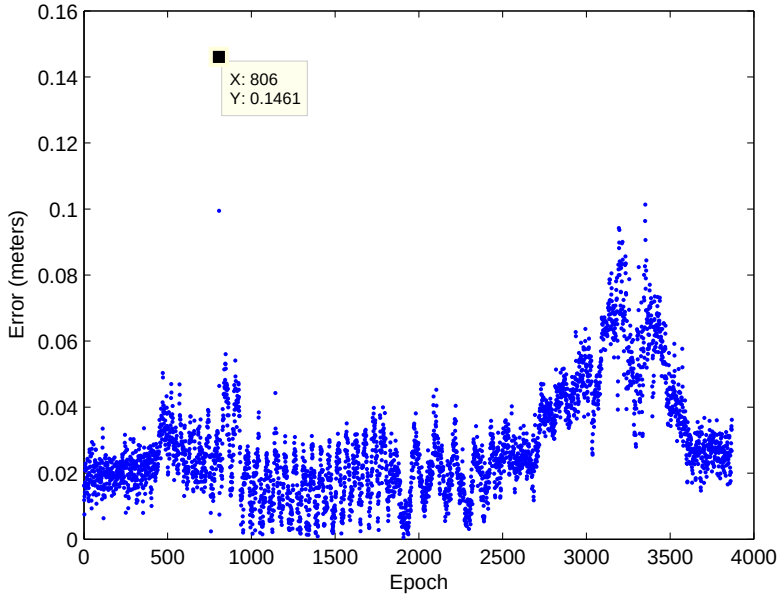

Figure 4.8: 3-D error for the road test using method 1 in early testing. Large spike corresponds to a incorrectly initialized ambiguity.

the maximum vertical error. Medium errors are between 33 and 66 percent of the maximum vertical error.

Looking at the three plots (Figures 4.11 and 4.12), it appears that the locations with large vertical errors correspond with areas that have sparse GPS positions in the vicinity. The turn in Figure 4.11 is a known location where the trajectories pass very close to the end of the surface grid. Using a larger number of GPS points that more completely cover the test terrain might allow the creation of a more accurate surface grid. This could possibly reduce the variations in the vertical direction.

4.3 Simulation Results

Simulations will be used to gain more insight into the differences between the different surface constraint methods. The simulations are created so that the iterative process of each method is seen. Unless otherwise specified, the ambiguity search process is skipped in order to focus on the impact of the various surface constraint

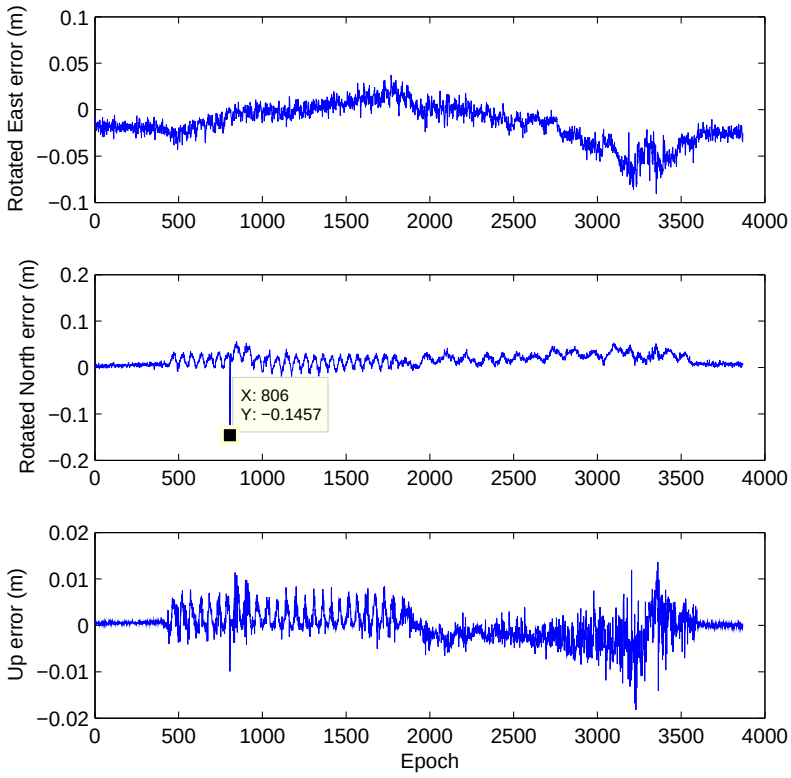

Figure 4.9: Error components for the road test using method 1 in early testing. Large spike corresponds to a incorrectly initialized ambiguity.

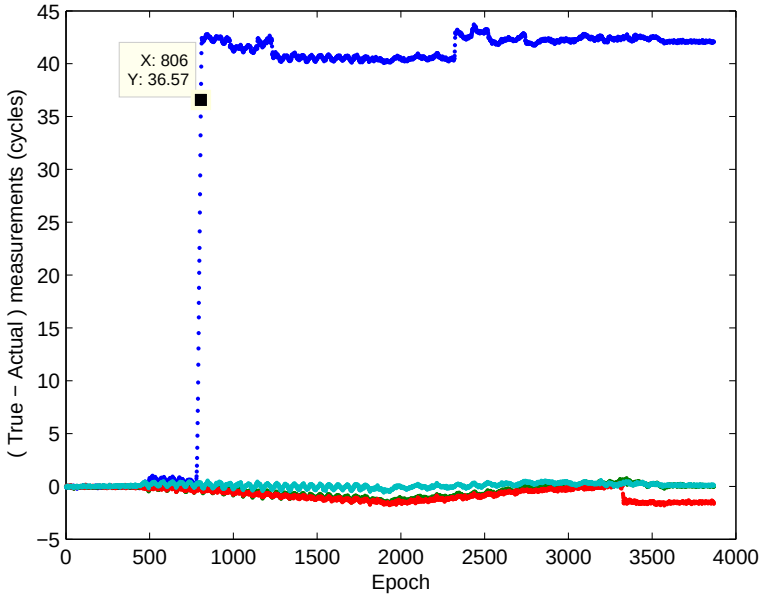

Figure 4.10: True measurement residuals for the road test. True measurement residuals are the difference between the actual measurements and what the measurements are calculated to be using the truth trajectory.

methods on positioning solutions. The ambiguities are initialized to the true values (known, because it is a simulation). This eliminates any complications in comparing the different methods. Isolating a particular characteristic of the methods is the goal of each simulation. In many cases, perfect measurements will also be used. This will allow any fundamental differences to be more easily seen. Adding noise to the measurements can mask some differences in the methods. Each simulation will be discussed and the results using each method will be discussed at the same time. This will allow the differences between the algorithms to be easier to compare.

4.3.1 Flat Simulation. A simple flat plane is simulated first. Perfect measurements will be used initially to demonstrate how the operation of each method in an environment with surface dynamics is similar. The surface grid, truth positions, and measurements are all artificially created. Each method uses the same information for its calculations.

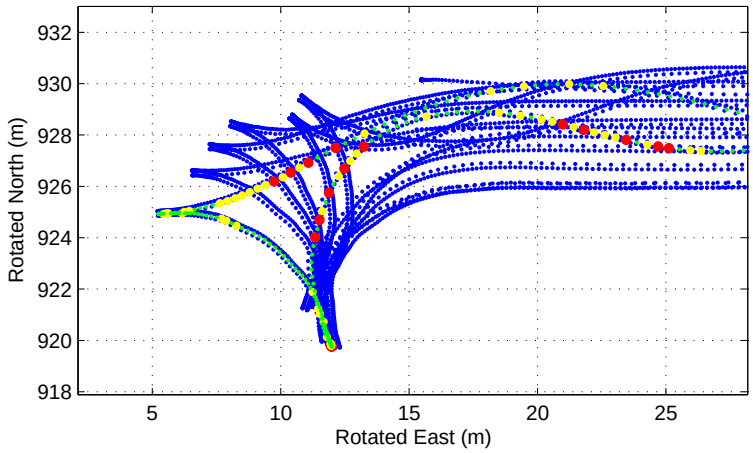

Figure 4.11: Vertical errors plotted along with grid trajectories in a turn. The larger points are medium vertical errors (also yellow), and large vertial errors (also Red).

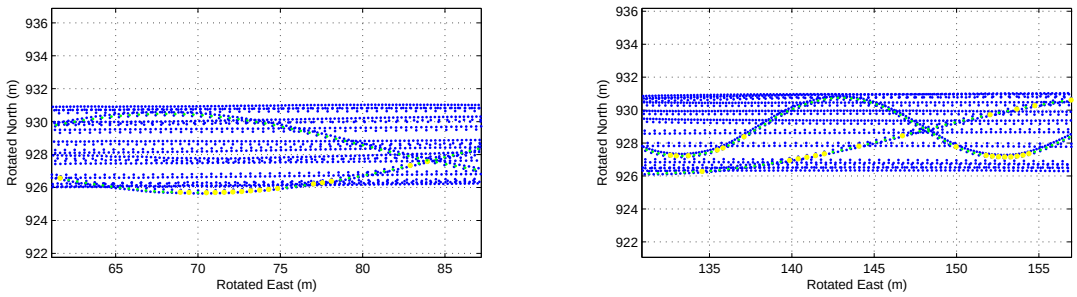

(a) (b)

Figure 4.12: The larger points are medium vertical errors (also yellow), and large vertial errors (also Red).
(a) Section in the middle of track
(b) A second plot of another section in the middle of the test run

Table 4.2: Average number of iterations assuming a flat surface.

Method #	Average number of iterations
1	3.00
2	3.11
3	2.99
4	3.00
5	2.98

4.3.1.1 Perfect Measurements. Initially, no measurement noise or tropospheric delay has been added to the measurements. The truth trajectory is made up of 100 points at the origin. The simulation selects 100 random poins within a 40 by 40 meter square around the origin. These points will be used as the initial points for the each time epoch. The solution errors for all five methods are plotted in Figure 4.13. The errors are all very small (on the order of 10^{-8} meters). The differences between the solutions is really negligible - all the methods have essential found the correct solution. The number of iterations is also a key indicator of performance. As expected, in this flat scenario there is little difference between the various algorithms. The average number of iterations is shown in Table 4.2. All the methods took approximately 3 iterations to find the solution.

4.3.1.2 Measurement Noise. The previous simulation was repeated, but this time measurement noise was added to the carrier-phase measurements. White, Gaussian noise with a standard deviation of 1/12 cycles (1 cm error) is added to the measurements. The results are shown in Figure 4.14. The error is now on the order of a centimeter, which is to be expected based upon the noise applied to the measurements. The methods all still take an average of approximately 3 iterations to calculate the final solution. The methods all perform nearly the same even with noise added to the measurements.

4.3.2 Hills Simulation. Simulation of a hill at the origin is a basic test of the methods. Several different simulations can be created with the same surface in-

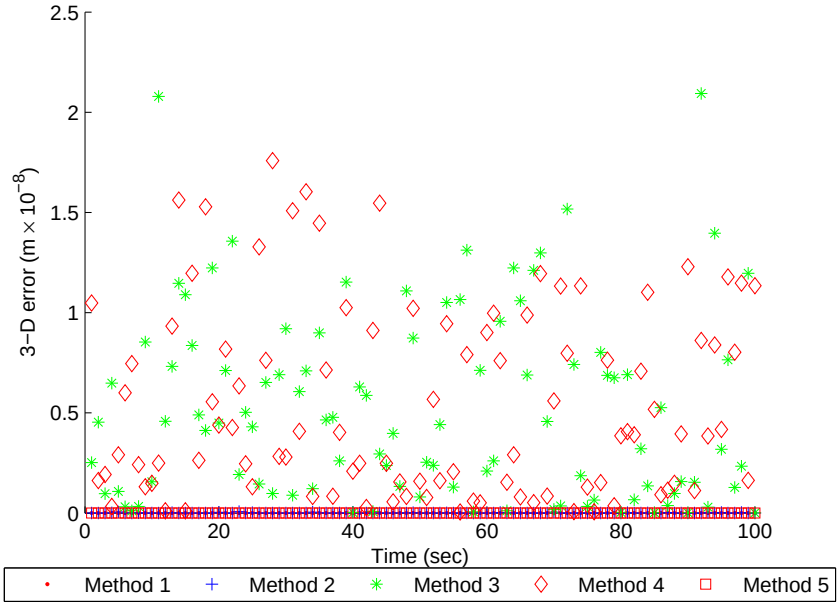

Figure 4.13: 3-D error for the flat simulation with no noise.

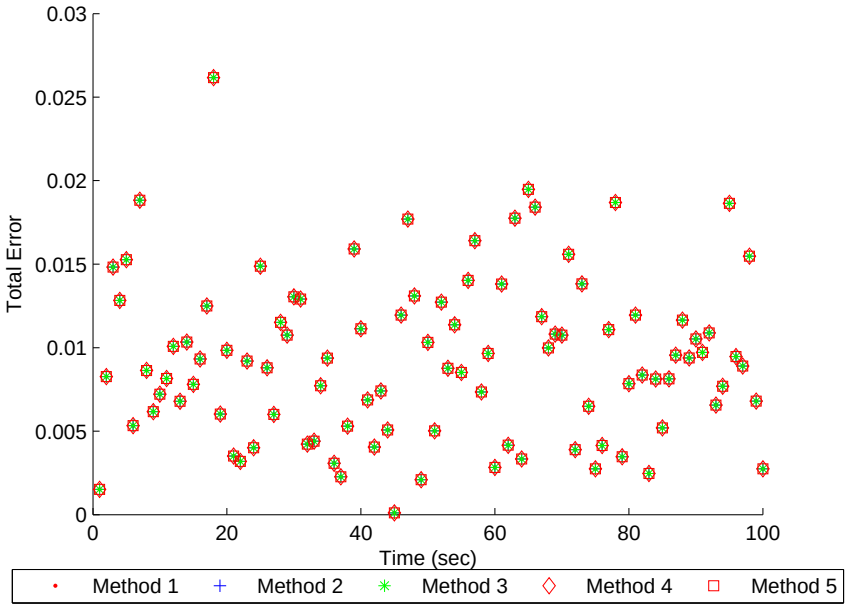

Figure 4.14: 3-D error for the flat simulation with noise added.

Table 4.3: Locations of pseudolites in ENU frame with the receiver at the origin.

PRN #	East (m)	North (m)	Up (m)
1	-100	100	30.5
2	100	-100	29.5
3	-100	-100	30.0
4	100	100	30.0

formation. It is interesting to see how each method behaves when trying to estimate a position on the hill starting from different initial positions. Alternatively, the methods can be tested using the same initial condition while trying to estimate different positions on the hill. These different simulations are aimed at discovering if different methods are better for different types of surfaces.

4.3.2.1 Single Truth Location/Perect Measurements. The hill that will be used as surface will be 20 meters tall with a footprint of roughly 20 x 20 meters. The locations of the pseudolites are given in Table 4.3.

Perfect measurements will be used to estimate the position of the top of the hill. To see if any algorithms are more or less prone to poor initial starting positions, 100 different initial positions will be simulated. The results are shown in Figure 4.15. While the errors are on the order of micrometers, it is interesting to note that method 5 has the lowest final position errors. Method 5 also has the lowest number of iterations. The number of iterations at each time and for each method are shown in Figure 4.16. Method 5 consistently takes five iterations to converge, while the other methods take close to 6 and 7 iterations on average.

Method 5 seems to be superior to the other methods of aiding. This could be due to its ability to incorporate the information contained in the surface topography more efficiently. All of the other methods described in this research incorporate the height information into the solution process in a delayed manner.

For example consider Method 1. The height is constrained to lie on the surface, but the height is found using the horizontal components from the previous iteration.

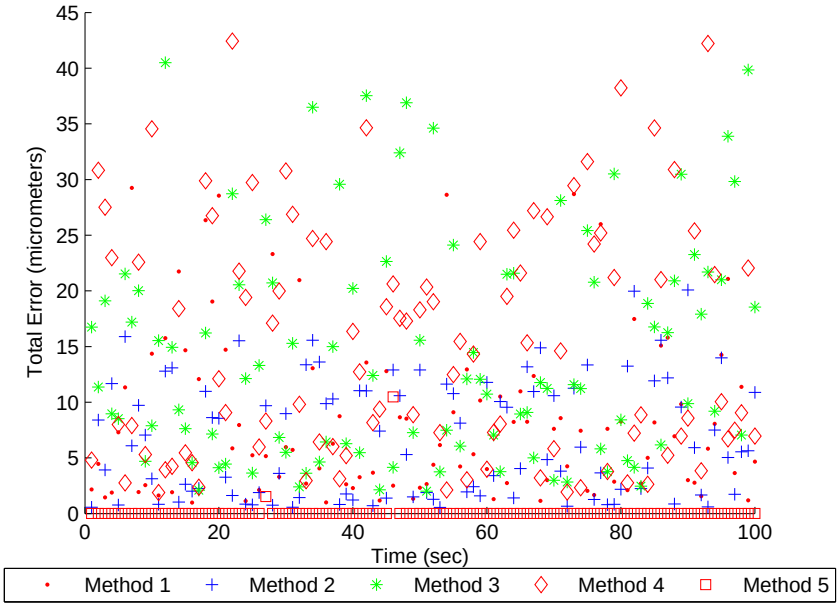

Figure 4.15: 3-D error for the hilltop simulation with no noise.

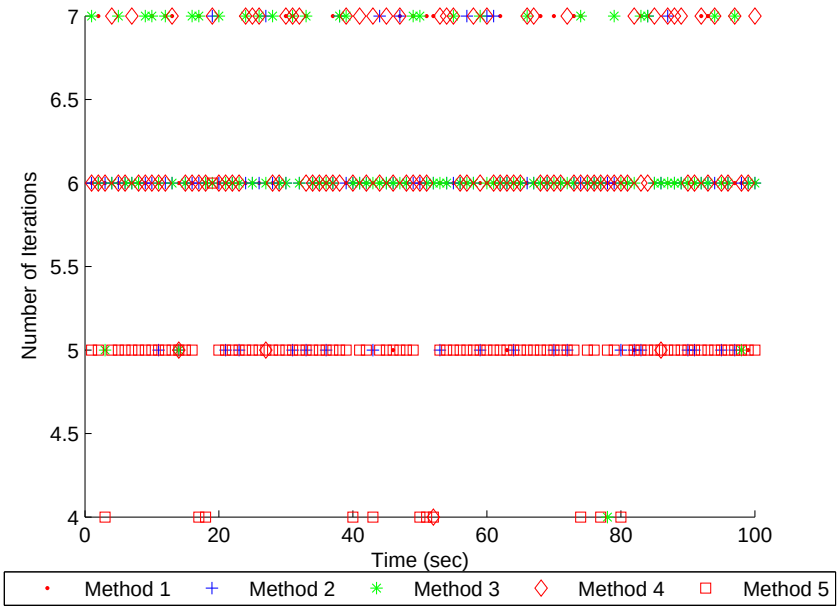

Figure 4.16: Number of iterations until convergence for the hilltop simulation.

This does not effectively constrain the height of the current solution to where the solution is going to be. As a result, the iteration must converge in steps. In cases of near horizontal surfaces, the effect of this constraint issue is not seen. When a surface with a higher slope is introduced, problems occur. On a surface with a high slope, a small horizontal change causes a large change in the height. This can require more iterations for convergence and possibly lead to a larger final error.

Method 5 is the only method that constrains the solution to a plane that is tangent to the surface topography. In the case of a surface with a large slope, the solution is now being found in a plane that is rotated to align with the only possible direction of change - along the surface.

While the tangent plane may be good for steep slopes, it is pustulated that it may have convergence problems at the peaks of hills. If the peak of the hill is very sharp, a small change in the position would create a vastly different solution plane, causing the solution to oscillate about the peak without converging.

4.3.2.2 Single Initial Position. This simulation will better investigate the different algorithms ability to estimate positions at different locations on the hill. A single initial position is used for each time epoch, with 100 different truth positions scattered over the hill. To create a surface with higher slope, the hill height has been increased to 40 meters. Measurements are still considered with no errors.

Figure 4.17 illustrates the errors in the final positions estimated by each method. It is obvious that method five has outperformed the others. Looking at the average number of iterations in Table 4.4, there is not as strong a separation in the number of iterations as shown when estimating the top of the hill.

4.4 Summary

This section has shown the results of the real road test and several simulations. The road test has proven that centimeter level accurate solutions can be obtained using the algorithms developed in this research. Analysis of the real data has shown

Table 4.4: Average number of iterations in hill simulation assuming common initial positions.

Method #	Average number of iterations
1	3.52
2	5.07
3	3.17
4	3.17
5	3.44

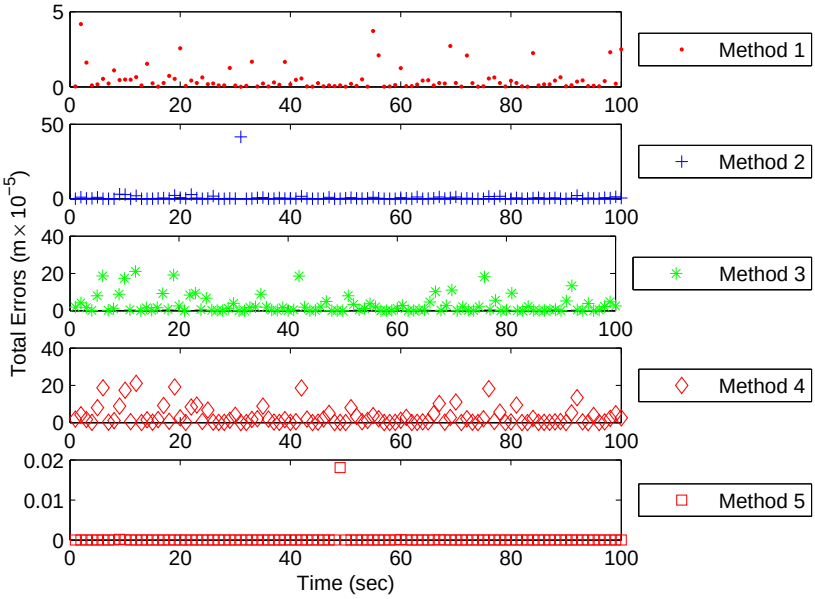

Figure 4.17: 3-D error for the hill simulation with no noise and common initial positions.

the need for better cycle slip detection methods. Multiple simulations have shown the superiority of the tangent plane constraint method.

V. Conclusion

5.1 Overview

This research aims at developing different methods of aiding and addressing the vertical deficiencies that occur in position estimation using pseudolite-based reference systems.

In a ground-based reference system using pseudolites, the vertical deficiency can be much greater than in GPS cases. The use of height constraints is a viable method of aiding the navigation solution.

Height constraints for aiding navigation solutions have been used in marine environments in past research [17, 23, 27]. This is valid since the height of the sea and thus the receiver can be well known. In cases of navigating on a changing ground topography, knowledge of the surface height can be attained from available surface grids (DTED), or from surveying the terrain manually. This knowledge is not applicable as in the marine case. Finding the height from a surface grid requires the knowledge of the horizontal position components.

Five different methods have been developed and discussed in this research.

- Method 1: Constrain the solution to the horizontal plane and use the horizontal solutions to find the height of the known surface at those coordinates.
- Method 2: Estimate in three dimensions using a pseudo-measurement to constraining the height. The height constraint will change during the iteration process as the pseudo-measurement is found by projecting the nominal solution onto the known topography.
- Method 3: Use the method of Singular Value Decomposition to remove the least observable position state from the state space. This is done at every epoch.
- Method 4: Again use SVD approach, but instead use it on the entire batch process. This will remove any states that are poorly observable.

- Method 5: The solution is constrained to lie on a plane that is tangent to the known surface topography. This plane will be tangent at the current solution and will update during the iteration process.

These methods were used to estimate the position of a receiver in a real road test as well as in simulation.

5.2 Conclusions

The road test was conducted as a proof of concept of using a pseudolite-based sysem as well as for generation of real measurement data. This data can be used for the estimation of real error parameters such as residual tropospheric error and transmitter position errors. The research used a batch ILS estimation process to calculate the floating point ambiguities. Using the above methods it has been shown that sub-decimeter-level accuracy is attainable with the current system. Future developments in both Locata hardware and integer ambiguity resolution algorithms have the potential for even higher levels of accuracy.

The cycle slip detection method of using SNR measurements has been analyzed and found lacking. The shortcomings of the this method have been shown decisively. Tropospheric correction has been done using a new algorithm that can handle low elevation transmitters. The residual tropospheric delay is present, but has not been a focus of modelling in this research.

The methods for aiding the solution process using knowledge of the surface topography were developed and then compared using multiple simulations. A flat horizontal surface allows all the methods to behave the same. Their identical performance in the presence of perfect measurements and noisy measurements illustrates the idea that these methods are not needed for a case when the height of the receiver is known accurately (as in marine cases).

Various simulations using a single hill were conducted. The effect of a higher sloped surface and the addition of noisy measurements indicated the inadequacy of using a pseudo-measurement for incorporating the height constraint.

Using a simulation focused on attaining solutions at different locations on a hill, it was found that constraining the solution to a plane tangent to the surface of the hill allowed a more accurate solution to be found.

While the simulations conducted barely scratch the surface of possible tests that can be conducted, the method of constraining the solution to lie on a tangent plane to the known surface has shown the best convergence in terms of accuracy and number of iterations. This method incorporates the knowledge of the surface in the most efficient manner.

5.3 Contributions

The following contributions have been made by this research.

- The largest contribution of this research is the development of the 5 different methods for aiding the height determination in pseudolite-based reference systems. These methods can be used to take advantage of the known surface topography of a test area.
- Development of a batch ILS approach to determine absolute position using a pseudolite network and carrier-phase measurements.
- Characterizing the errors involved in cycle slip detection of LocataLite measurements from SNR values. Using post processed data with a known truth trajectory it can be shown that this method is not sufficient for detection of cycle slips, which is crucial for attaining precise solutions.
- Development of various simulations for comparing different methods of height aiding. These simulations are important for understanding the tradeoffs in using each method.

- Determination of the tangent plane transformation method as the best method for aiding the height determination in a pseudolite-based reference system.

5.4 Recommendations

This research focused on aiding a batch least-squares estimation algorithm in determining the position of a receiver using a pseudolite-based reference system. The need for such a pseudolite-based reference system is great and further research is needed to bring this into final stages of development. Recommendations for further research are given below.

- Further investigation into the strengths and weaknesses of the different methods developed in this research. This motivates the optimization of the algorithm code so accurate comparison of convergence times can be done.
- Implement the methods developed in this research in real world tests that contain more varied surfaces. The road used in this test was nearly flat and therefore all the methods performed similarly. A more dynamic test surface will better explore the differences in the methods in a real world environment.
- More investigation of the ability of the batch least-squares process in estimating system errors such as residual tropospheric error and pseudolite position errors. The focus of this research was on development of the different surface constraint methods. More potential lies in using the batch process to estimate some of the system errors that might be more observable using a batch process.
- Instead of creating a surface grid using GPS survey points, investigate other methods of generating a map of the topography. Using Digital Terrain Elevation Data (DTED) information is an obvious example that could be researched.
- Investigate the use of implementing these method for use in cases other than pseudolite-based systems. In marine situations, height constraints are commonly used, since the height is well known. The use of aiding a GPS solution

with a known topography surface (DTED for example) could be used to boost accuracy and robustness issues when GPS geometry is poor.

- Using multiple methods in the search process may allow for more accurate solutions. Given a trajectory that contains areas of high and low surface dynamics, different methods may be converge quicker or attain better accuracy in different locations. Combining methods could take advantage of the strengths and weaknesses of each aiding method.

Bibliography

1. Barnes, J., C. Rizos, M. Kanli, A. Pahwa, D. Small, G. Voigt, N. Gambale, and J. Lamance. "High Accuracy Positioning using Locata's Next Generation Technology".

2. Barnes, Joel, Chris Rizos, Mustafa Kanli, David Small, Gavin Voigt, Nunzio Gambale, Jimmy Lamance, Terry Nunan, and Chris Reid. "Indoor Industrial Machine Guidance Using Locata: A pilot study at BlueScope Steel." *Proceedings of the 2004 Annual Meeting of the U.S. Institute of Navigation*. Dayton, OH, June 2004.

3. Barnes, Joel, Chris Rizos, Mustafa Kanli, David Small, Gavin Voigt, Nunzio Gambalie, and Jimmy Lamance. "Structural Deformation Monitoring using Locata". *Proceedings of the 2004 International Symposium on Engineering Surveys for Construction Works and Structural Engineering*. Nottingham, UK, June 2003.

4. Barnes, Joel, Chris Rizos, Jinling Wang, David Small, Gavin Voigt, and Nunzio Gambale. "High precision indoor and outdoor positioning using LocataNet". *Prodeedings of the 2003 International Symposium on GPS/GNSS*. Toyko, Japan, November 2003.

5. Barnes, Joel, Chris Rizos, Jinling Wang, David Small, Gavin Voigt, and Nunzio Gambale. "LocataNet: A new positioning technology for high precision indoor and outdoor positioning". *Proceedings of the 2003 International Technical Meeting of the Satellite Division of the U.S. Institute of Navigation*. Portland, OR, September 2003.

6. Barnes, Joel, Chris Rizos, Jinling Wang, David Small, Gavin Voigt, and Nunzio Gambalie. "Locata: the positioning technology of the future?" *Proceedings of the 2003 International Symposium on Satellite Navigation Technology Including Mobile Positioning and Location Services*. Melbourne, Australia, July 2003.

7. Blackman, Samuel and Robert Popoli. *Design and Analysis of Modern Tracking Systems*. Artech House, Norwood, Massachusetts, 1999.

8. Bouska, Terry J. *Development and Simulation of a Pseudolite-based Flight Reference System*. Master's thesis, Air Force Institute of Technology, March 2003.

9. Bouska, Terry J. and John F. Raquet. "Tropospheric Model Error Reduction in Pseudolite-Based Positioning Systems". *Proceedings of ION-GPS/GNSS 2003*. Portland, OR, September 2003.

10. Cobb, Stewart H. *GPS Pseudolites: Theory, Design, and Applications*. Ph.D. thesis, Stanford University, September 1997.

11. Dierendonck, A.J. Van. "Local Differential Tropospheric Delay Corrections", August 1997. Internal Memo for RTCA Special Committee 159 Working Group 4.

12. Jolliffe, I. *Principal Component Analysis*. Springer-Verlag, New York, NY, 2002.

13. Kwon, Young-Hoo. "Transformation Matrix". Internet Website, February 2006. Http://kwon3d.com/theory/transform/transform.html.

14. Lawrence, Robert S. "CIGTF Enhanced Precision Reference Systems", October 2004. Power Point Presentation.

15. Lee, Hung Kyu, Jinling Wang, Chris Rizos, Joel Barnes, Toshiaki Tsujii, and Ben K.H. Soon. "Analysis of Pseudolite Augmentation for GPS Airborne Applications". *Proccedings of the 2002 ION GPS*. Portland, OR, September 2002.

16. Misra, Pratap and Per Enge. *Global Positioning System Signals, Measurements, and Performance*. Ganga-Jamuna Press, Lincoln, Massachusetts, 2004.

17. Morley, T. and G. Lachapelle. "GPS Augmentation with Pseudolites for Navigation in Constricted Waterways". *Proceedings of the National Technical Meeting*. Santa Monica, CA, January 1997.

18. Press, W.H., S. A. Teukolsky, W. T. Vetterling, and B.P. Flannery. *Numerical Recipes in C*. Cambridge University Press, Cambridge, NY, 1992.

19. Raquet, John. "Class Notes to EENG 533". Air Force Institute of Technology.

20. Raquet, John. "Class Notes to EENG 633". Air Force Institute of Technology.

21. Raquet, John. "Optimal Rank Reduction of Design Matrix for Least Squares Estimation", October 1995. Written report at University of Calgary, Calgary, Alberta, Canada.

22. Raquet, John, G. Lachapelle, W. Qiu, C. Pelletier, T. Nash, F. B. Snodgrass, P. Fenton, and T. Holden. "Development and Testing of a Mobile Pseudolite Concept for Precise Positioning". *Navigaion: Journal of The Institute of Navigation*, 43(2), 1996.

23. Ryan, S., M. Petovello, and G. Lachapelle. "Augmentation of GPS for Ship Navigation in Constricted Water Ways". *Proceedings of the National Technical Meeting*. Long Beach, CA, January 1998.

24. Shockley, Jeremiah. *Estimation and Mitigation of Unmodeled Errors for a Pseudolite Based Reference System*. Master's thesis, Air Force Institute of Technology, March 2006.

25. Tascione, Thomas F. *Introduction to the Space Environment*. Krieger Publishing Company, Malabar, Florida, second edition, 1994.

26. Wang, J. "Pseudolite Applications in Positioning and Navigation: Progress and Problems". *Journal of Global Positioning Systems*, 1(1):48–56, 2002.

27. Weisenburger, S. and M. E. Cannon. "Performance Improvements Using Constraints in Marine OTF Ambiguity Resolution". *Proceedings of the National Technical Meeting*. Santa Monica, CA, January 1997.

REPORT DOCUMENTATION PAGE

Form Approved
OMB No. 0704–0188

1. REPORT DATE *(DD–MM–YYYY)*	2. REPORT TYPE	3. DATES COVERED *(From — To)*
23–03–2006	Master's Thesis	Sept 2004 — Mar 2006

4. TITLE AND SUBTITLE

Methods For Aiding Height Determination
In Pseudolite-Based Reference Systems
Using Batch Least-Squares Estimation

5a. CONTRACT NUMBER

5b. GRANT NUMBER

5c. PROGRAM ELEMENT NUMBER

6. AUTHOR(S)

John Harold Robert Amt

5d. PROJECT NUMBER

5e. TASK NUMBER

5f. WORK UNIT NUMBER

7. PERFORMING ORGANIZATION NAME(S) AND ADDRESS(ES)

Air Force Institute of Technology
Graduate School of Engineering and Management (AFIT/EN)
2950 Hobson Way
WPAFB OH 45433-7765

8. PERFORMING ORGANIZATION REPORT NUMBER

AFIT/GE/ENG/06-03

9. SPONSORING / MONITORING AGENCY NAME(S) AND ADDRESS(ES)

746th Test Squadron AFMC
Terry J. Bouska, Capt, USAF 1644 Vandergrift Rd
Holloman Air Force Base, NM 88330
DSN: 349-1772 Email: Terry.Bouska@46tg.af.mil

10. SPONSOR/MONITOR'S ACRONYM(S)

11. SPONSOR/MONITOR'S REPORT NUMBER(S)

12. DISTRIBUTION / AVAILABILITY STATEMENT

Approval for public release; distribution is unlimited.

13. SUPPLEMENTARY NOTES

14. ABSTRACT

There are many situations in which GPS is either unable to provide the desired level of accuracy or is unavailable. Use of a pseudolite-based reference system for navigation can be a means for positioning during these times. While there are advantages in using a pseudolite-based reference system, there are still implementation issues and deficiencies that must be addressed. In many cases a pseudolite system with ground based transmitters has difficulty in determining the height of the receiver accurately. This is due to the poor vertical observability inherent in the geometry of the system. A common approach in naval applications for solving the problem of poor vertical observability is to use a height constraint, which is well known when travelling on a surface of water. For a ground-based vehicle, knowledge of the surface topography can be obtained, but cannot be readily used in the same manner as marine cases, since the height is often a varying function of position.
This research investigates and develops five methods of incorporating the known surface topography in a non-linear batch

15. SUBJECT TERMS

pseudolites, Global Positioning System, GPS, DGPS, Batch Least Squares Estimation, Least Squares Estimation, Height Constraint

16. SECURITY CLASSIFICATION OF:			17. LIMITATION OF ABSTRACT	18. NUMBER OF PAGES	19a. NAME OF RESPONSIBLE PERSON
a. REPORT	b. ABSTRACT	c. THIS PAGE			Raquet, John F., Ph.D., (ENG)
U	U	U	UU	105	19b. TELEPHONE NUMBER *(include area code)* (937) 255–3636, ext 4580